IN - 39810

JPL PUBLICATION 86-40

(MSAT-X REPORT No. 138)

P_ 72

Tone Calibration Technique: A Digital Signaling Scheme for Mobile Applications

Faramaz Davarian

September 15, 1986

NASA

National Aeronautics and
Space Administration

Jet Propulsion Laboratory
California Institute of Technology
Pasadena, California

Tone Calibration Technique: A Digital Signaling Scheme for Mobile Applications

Faramaz Davarian

September 15, 1986

NASA

National Aeronautics and
Space Administration

Jet Propulsion Laboratory
California Institute of Technology
Pasadena, California

ABSTRACT

Residual carrier modulation has conventionally been used in a communication link to assist the receiver with signal demodulation and detection. Although suppressed carrier modulation has a slight power advantage over the residual carrier approach in systems enjoying a high level of stability, it lacks sufficient robustness to be used in channels severely contaminated by noise, interference and propagation effects. In mobile links, in particular, the vehicle motion and multipath waveform propagation affect the received carrier in an adverse fashion. For example, both signal amplitude and phase (or frequency) suffer from random fluctuations known as the random AM and random FM, respectively. These random fluctuations make it difficult for the receiver to successfully track the phase of the carrier for coherent demodulation, conduct automatic gain control for keeping the average signal level at a constant level, etc.

This publication describes a residual carrier scheme that uses a pilot carrier to calibrate a mobile channel against multipath fading anomalies. The benefits of this scheme, which is known as the tone calibration technique, are: (1) coherent signal demodulation in spite of carrier phase fluctuations, (2) removal of fading induced error floor, and (3) insensitivity to Doppler and small frequency errors. Although the scheme described in this publication is a generic digital modulation/demodulation technique, for the sake of compactness, only the case of QPSK is addressed.

Analytical as well as experimental results are presented. A brief study of the system performance in the presence of implementation anomalies is also given. It is shown that the system architecture calls for digital implementation and further testing of the transceiver.

ACKNOWLEDGMENT

CONTENTS

APPENDIX

<u>Figures</u>

I. INTRODUCTION

The increased popularity of mobile communications in recent years has provided a strong incentive for research and development in this area. It is generally believed that the use of new advancements in microelectronics and digital information transmission techniques would help make mobile communications more economical. Moreover, new services such as the satellite-aided mobile communications are banking on technological advancements for cost effective exploitation of new market areas.

Traditional mobile communications services have been generous with precious channel resources of spectrum and power. Presently, the most common method of mobile communications is a technique known as the narrowband FM which uses 25- or 30-kHz channel spacing in a frequency division multiple access (FDMA) system. Although narrowband FM is credited with robustness and simplicity, it is very inefficient in the use of frequency.

The market growth and the increase in user expectations have resulted in more sophisticated, modern, mobile networks. The control of such complex systems and the user needs have made digital signal transmission a necessity. Digital signaling is also more economical than conventional FM techniques. In general, digital communications is required in three areas: network control and management, alphanumeric (data) signal transmission, and digital voice. Unfortunately, conventional digital signaling schemes are not very effective in narrowband mobile channels. Most known techniques suffer from one or more shortcomings. For example, due to the difficulty the receiver has in satisfactorily recovering the carrier phase, coherent signaling is unsuitable for multipath fading links. Realizing these shortcomings, the designers of future mobile networks are investigating new approaches to signal transmission and reception. The primary considerations given, especially for satellite-aided systems, are: (1) robustness, i.e., easy recovery from deep fades and fast response to bursty signals, (2) narrow spectral occupancy, and (3) good power performance. For mobile terminal cost reduction, constant envelope property is also desirable.

Carney and Linder (Ref. 1) were the first to experiment with digital FM radios using noncoherent receivers where some degree of premodulation filtering is performed for signal bandlimiting. They have succeeded in partially meeting the first two considerations, robustness and narrow bandwidth, but not the third one, power efficiency. An alternative to digital FM is a technique known as GMSK, which has become increasingly popular in recent years (Ref. 2). GMSK is, in essence, minimum shift keying (MSK) with Gaussian filtering of the baseband signal. Simon and Wang (Ref. 3) have performed an extensive study of a two-bit differential detector for GMSK and have shown means of optimizing receiver parameters in the presence of fading. Later, the feasibility of differential GMSK as a potential digital signaling scheme for mobile satellite applications was demonstrated at the Jet Propulsion Laboratory (Ref. 4). GMSK is superior to digital FM both in spectrum and power performance, but it is more sensitive to Doppler and frequency offset than digital FM. Nevertheless, both digital FM and GMSK suffer from a large error floor in the presence of multipath fading when transmission rate is low, i.e., less than 16 kbps.

Empirical (Ref. 5) as well as analytical studies indicate that signal propagation in a multipath environment results in random amplitude and phase fluctuations. The rate of these random AM and PM modulations is proportional to the vehicle speed and the carrier frequency, hence the incident Doppler. In the 800-MHz band, a Doppler value close to 100 Hz is not uncommon. In principal, it is desirable to reduce the effect of these time-dependent channel impairments by means of adaptive calibration techniques. However, due to the high-rate variations of these impairments, traditional equalization schemes are not effective. Therefore, conventional digital radios suffer from two limitations:

(1) Due to the random FM present in mobile links, narrow-band digital communication suffers from a link-dependent error floor. This irreducible error rate is a function of Doppler and data rate.

(2) Due also to the random FM, coherent signal demodulation in low symbol rate links is impractical. Noncoherent or differentially coherent techniques such as differential M-ary phase shift keying (MPSK) are inferior to their coherent counterpart by about 3 dB.

Therefore, to remedy the above limitations, it appears advantageous to transmit a pilot tone along with the signal to continuously calibrate the channel[1]. This pilot tone can be extracted at the receiver to perform two functions simultaneously, combat the fading induced impairment, and perform coherent demodulation. To achieve both these goals, the calibration tone must fulfill three requirements. First, the relative position of the tone in the channel must be carefully selected such that the tone and the accompanying signal experience the same distortion, including propagation effects and hardware imperfection. Second, the calibration tone has to coincide in frequency and phase with the carrier if coherent demodulation is desired. Third, for power conservation it is also desirable to use only a small portion of the total power for transmission of the pilot tone.

Because the pilot tone and the data-bearing signal must share the same channel, it is necessary to create a spectral null at the appropriate location (or locations if more than one tone is used) to prevent self-interference. Nulling of the spectrum can be performed by the encoding of data such that the DC component of the signal is suppressed. A number of schemes exist which can create the desired null, including correlative techniques and the Miller and balanced codes (see the appendix). A spectrally efficient scheme proposed by McGeehan and Bateman (Ref. 6), which creates a spectral gap without encoding, can also be employed. Each of these encoding methods has its own advantages and drawbacks. However, since it is not the intention of this publication to treat the encoding issue, no further discussion of this topic will be made. For the rest of this publication it will be assumed that Manchester encoding is used. It is worth mentioning at this point that in the case of a one-dimensional signal structure, the pilot can be transmitted 90 degrees out of phase with respect to the carrier, avoiding the need for spectrum processing (Refs. 7 and 8).

---

[1]A dual-tone system is also possible.

This publication describes a study whose goal was to develop a digital signaling technique that is insensitive to multipath-fading-induced phase distortion. The proposed scheme achieves its goal by continuous calibration of the fading channel. Since the calibration is performed via a pilot tone (or tones), the approach is called the Tone Calibration Technique (TCT).

Although TCT is a generic scheme, only the case of QPSK is considered here because the extension of the technique to other signals is straight forward. The transmitter block diagram is illustrated in Fig. 1. The source output is split into in-phase and quadrature streams. A zero-DC encoding technique, e.g., Manchester, is applied to create the intended null at the center of the spectrum. Next, pulse-shaping filters may be introduced for the sake of signal bandlimiting. Finally, quadrature modulation along with carrier (tone) insertion is performed.
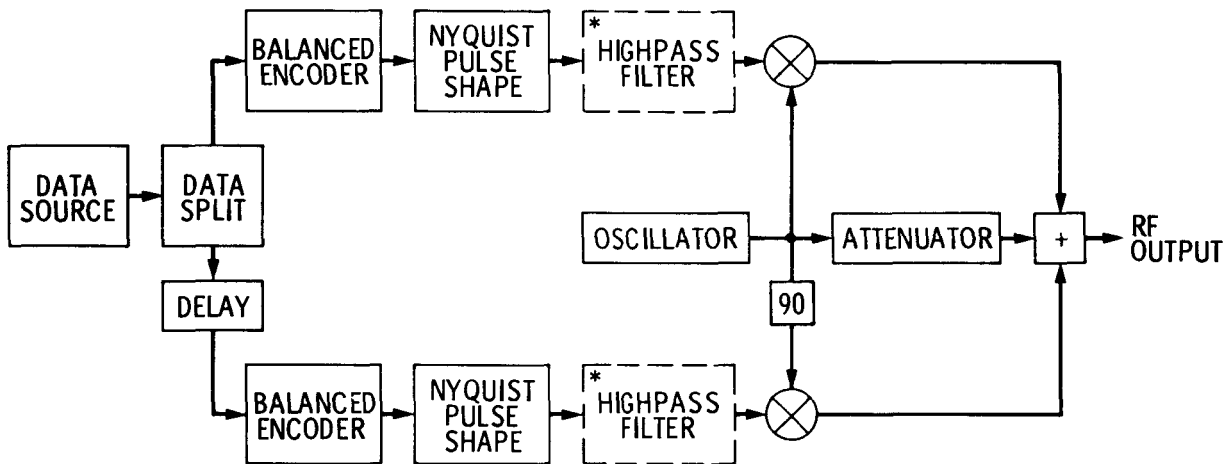
*this filter may be used to reduce self-interference

Figure 1.   Transmitter block diagram.

The TCT receiver may be implemented at IF or baseband. Although the baseband version has practical advantages, the IF format is easier to analyze. Since the pilot tone can be used as a reference for coherent demodulation, a TCT receiver does not require a carrier tracking loop. The in-phase portion of a single-tone receiver with IF implementation is illustrated in Fig. 2. Conceptually, this receiver is simple. For pilot selection, a pilot bandpass filter (PBPF) is used, followed by a calibration subsystem that was first proposed by Leland and Sollenberger (Ref. 9) and has been used by McGeehan and Bateman in analog single-sideband radios (Ref. 10). The purpose of this subsystem is to create a waveform with an amplitude inversely proportional to that of the received pilot without affecting the phase. This subsystem is necessary to minimize the received signal dynamic range; it does, however, complicate the receiver. A compromise may be achieved by replacing the calibration system by a limiter, which is less complex. The mixer in Fig. 2
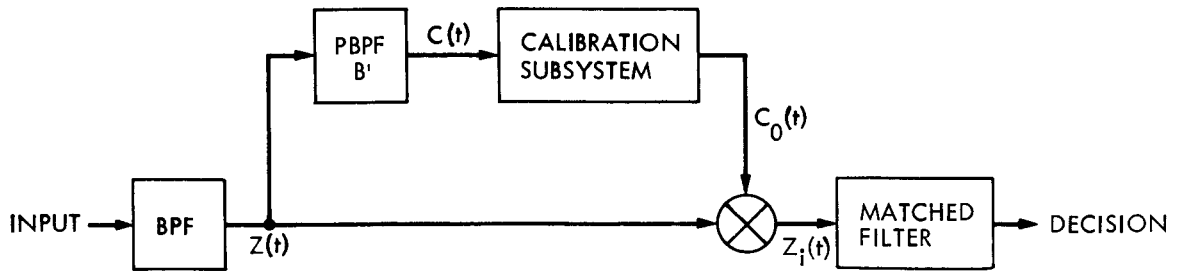
Figure 2.   Receiver block diagram for the in-phase signal component.

performs the demodulation and phase correction operations simultaneously. The demodulated signal is subsequently detected by a matched filter. Note that the predetection bandpass filter (BPF) is only for noise bandlimiting and has no effect on the signal.

Section II provides an analysis of the receiver, and numerical results are given in Section III. The baseband implementation is discussed in Section IV. Some remarks are provided in Section V. Construction of the transmitter is described in Section VI, and experimental results are given in Section VII.

II. MATHEMATICAL FORMULATION AND NOISE ANALYSIS

A. IDEAL CALIBRATION

As mentioned earlier, the propagation effects in a multipath fading channel can be modeled by random AM and PM fluctuations. Therefore, the received waveform (signal plus noise) at the output of BPF can be presented as (see Fig. 2)

$$Z(t) = P(t) + S(t) + N(t) \qquad (1)$$

where $P(t)$, $S(t)$, and $N(t)$ denote the pilot tone, signal, and noise components of the received waveform, respectively. These terms can be further expressed as

$$P(t) = aX_t \cos (\omega_o t + Y_t)$$

$$S(t) = \frac{A}{\sqrt{2}} X_t [S_i(t) \cos (\omega_o t + Y_t) + S_q(t) \sin (\omega_o t + Y_t)]$$

$$N(t) = N_i(t) \cos (\omega_o t) + N_q(t) \sin (\omega_o t)$$

In the first of the above set of equations, $a^2/2$, X_t, Y_t, and ω_o denote the average pilot tone power, random amplitude modulation, random phase modulation, and carrier angular frequency, respectively. Both X_t and Y_t are induced by fading. In the absence of fading, $X_t = 1$ and Y_t becomes a constant unknown phase. In the second equation, $A^2/2$ denotes the quadriphase modulated signal power, and $S_i(t)$ and $S_q(t)$ denote the in-phase and quadrature data-bearing signals, respectively. The last equation represents the bandpass white Gaussian noise with $N_i(t)$ and $N_q(t)$ being two independent baseband Gaussian noise terms having power density N_o.

In the following, only an analysis of the in-phase portion of the receiver will be presented. It is assumed that the receiver bit error probability is equal to an individual channel bit error probability, since the in-phase and quadrature channels are balanced. The receiver bit error probability as a function of E_T/N_o will be determined, where E_T is the total bit energy given by

$$E_T = \frac{a^2/2 + A^2/2}{R_b}$$

with R_b denoting the bit rate. Assuming B' is the bandwidth of PBPF, it will be shown that R_b/B' is an important link parameter.

The waveform at the output of PBPF can be written as

$$C(t) = aX_t \cos (\omega_o t + Y_t) + N_i'(t) \cos \omega_o t + N_q'(t) \sin (\omega_o t) \qquad (2)$$

where $N_i'(t)$ and $N_q'(t)$ are independent baseband Gaussian noise processes bandlimited to $B'/2$ and with power density N_o. The above equation can be presented in polar form as

$$C(t) = \rho(t) \cos [\omega_o t + Y_t + \Theta(t)] \qquad (3)$$

where $\rho(t)$ denotes the pilot tone envelope and $\Theta(t)$ is a phase modulation due to thermal noise. For the following analysis we assume perfect delay equalization of receiver filters to allow timely amplitude and phase correction. A treatment of problems related to the mismatching of the delays can be found in Ref. 10. The output of the calibration subsystem in Fig. 2 can be presented by

$$C_o(t) = \frac{1}{\rho(t)} \cos [\omega_o t + Y_t + \Theta(t)] \qquad (4)$$

Signal demodulation will result in the following baseband waveform (ignoring the double frequency term):

$$Z_i(t) = Z(t) \times C_o(t) = \frac{AX_t}{2\sqrt{2}\rho(t)} \{S_i(t) \cos [\Theta(t)] - S_q(t) \sin [\Theta(t)]\}$$

$$+ \frac{1}{2\rho(t)} \tilde{N}(t) + \frac{1}{2} \qquad (5)$$

where

$$\tilde{N}(t) = \tilde{N}_i(t) \cos [Y_t + \Theta(t)] - \tilde{N}_q(t) \sin [Y_t + \Theta(t)] \qquad (6)$$

with $\tilde{N}_i(t) = N_i(t) - N_i'(t)$ and $\tilde{N}_q(t) = N_q(t) - N_q'(t)$. $\tilde{N}_i(t)$ and $\tilde{N}_q(t)$ are independent white Gaussian noise processes with a spectral null at the origin and a null width of $B'/2$. The noise process $\tilde{N}(t)$ is Gaussian and white over the range of signal frequencies. The data-bearing signal energy about the origin is very small due to the Manchester encoding of data. Thus, the power density of $\tilde{N}(t)$ is essentially N_o. At this point a few clarifying comments should be made on this noise process. The underlying assumption here is that the bandpass noise process of Eq. (1) can be decomposed into two spectrally disjoint portions: a portion that falls within the bandwidth of PBPF, and one that is outside this region. The noise $\tilde{N}(t)$ is representing the contribution of the latter at the output of the demodulator. Since the resulting noise is phase-modulated by $Y_t + \Theta(t)$, its spectrum is not flat around the band boundaries. However, because the process $Y_t + \Theta(t)$ is of much narrower bandwidth than the signal $S_i(t)$, the power spectrum of $\tilde{N}(t)$ can be approximated as shown in Fig. 3.
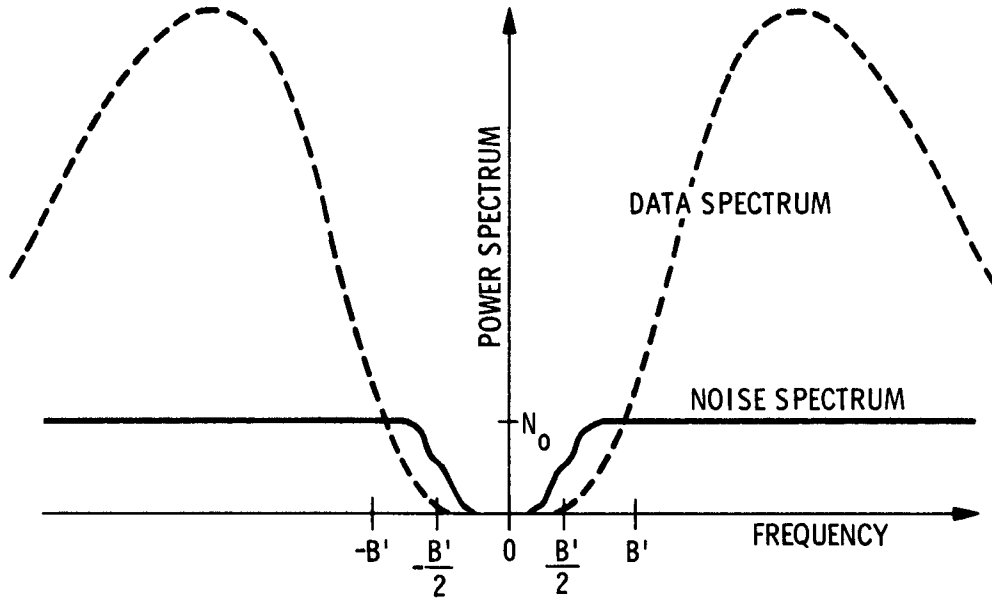
Figure 3. Power spectral density of noise $\tilde{N}(t)$.

For an ideally calibrated system, wherein B' is small, the noise in PBPF can be ignored. In this case, the observed signal, ignoring the DC term, is given by

$$Z_{i_{ideal}}(t) = \frac{A}{2\sqrt{2}a} S_i(t) + \frac{1}{2aX_t} \tilde{N}(t) \tag{7}$$

Since the process X_t varies slowly relative to the signal bit rate, X_t can be assumed to be a time-independent random variable. In fact, the 3-dB bandwidth of X_t equals twice the Doppler frequency (Ref. 11), whereas the data rate associated with $S_i(t)$ is 1200 to 32,000 bps (R_b = 2400 to 64,000 bps). Assuming $S_i(t)$ is an antipodal signal, the bit error probability associated with the TCT receiver is given by

$$P_e = \frac{1}{2} \int_0^\infty \text{erfc} (\sqrt{\Gamma}) \; p(\Gamma) d\Gamma \tag{8}$$

where $\Gamma = \gamma X_t$ and $\gamma = A^2/(2N_0 R_b)$. The mean E_b/N_0 over fading is denoted by γ (note that the mean bit energy equals 0.5 x A^2/R_b). Furthermore,

$$\text{erfc}(X) = \frac{2}{\sqrt{\pi}} \int_0^\infty \exp(-t^2) \, dt,$$

2-3

and p(Γ) denotes the probability density function of Γ. For Rayleigh and Rician multipath fading channels, this density function is readily available. For the Rayleigh case, it is given as

$$p(\Gamma) = \frac{1}{\gamma} \exp\left(-\frac{\Gamma}{\gamma}\right) \tag{9}$$

and for the Rician case, it becomes

$$p(\Gamma) = \frac{1 + K}{\gamma} \exp\left[-K - (1 + K)\frac{\Gamma}{\gamma}\right] I_o\left[2\sqrt{\frac{\Gamma}{\gamma}(1 + K)K}\right] \tag{10}$$

where K denotes the power ratio of the specular component to the diffused component and I_o denotes the modified Bessel function of order zero.

While Eq. (9) is widely used to model terrestrial links, Eq. (10) is best suited for describing satellite-aided mobile channels. For a large value of K, Eq. (10) represents a slightly fading channel wherein the received waveform is dominated by a steady signal. On the other hand, small values of K indicate a severely fading channel wherein the multipath components dominate. As K approaches zero, the channel assumes the Rayleigh characteristic of Eq. (9).

B. NONIDEAL CALIBRATION

For the nonideal case, when the noise in PBPF cannot be ignored, the demodulated signal is given by Eq. (5). The link error probability for this case is conditioned on two random variables, Γ and $\theta(t)$. Assuming that Γ is slowly varying over the bit period, this conditional error probability is given by (Ref. 12)

$$P_e|_{\Gamma,\theta} = \frac{1}{4} \text{erfc} [\sqrt{\Gamma} \cos \theta] + \frac{1}{8} \text{erfc} [\sqrt{\Gamma} (\cos \theta + \sin \theta)]$$

$$+ \frac{1}{8} \text{erfc} [\sqrt{\Gamma} (\cos \theta - \sin \theta)]. \tag{11}$$

Therefore, P_e can be evaluated as

$$P_e = \int\limits_{0}^{\infty} \int\limits_{-\pi}^{\pi} P_e|_{\Gamma,\theta} \, p(\theta|\Gamma)p(\Gamma)d\theta d\Gamma \tag{12}$$

The conditional probability density of $\theta(t)$, the phase modulation due to thermal noise at PBPF, is given by (Ref. 13)

$$p(\theta|\Gamma) = \frac{e^{-\delta\Gamma}}{2\pi} + \frac{\sqrt{\delta\Gamma} \cos \theta \exp [-\delta\Gamma \sin^2 \theta]}{2\sqrt{\pi}} [2 - \text{erfc} (\sqrt{\delta\Gamma} \cos \theta)] \qquad (13)$$

where $\delta = r\, R_b/B'$ and $r = a^2/A^2$. As mentioned earlier, $R_b/B' \gg 1$.

The performance of coherent receivers strongly depends on the stability of the recovered carrier phase. In the present system, Eq. (13) illustrates the spreading of this phase. Clearly, the phase stability is improved if $\delta\Gamma$ is increased. Parameter δ depends on two factors R_b/B' and r. For fixed R_b/B', r can be increased by allocating more power to the pilot tone. This will, in turn, reduce the phase noise described by Eq. (13), resulting in a lower receiver error probability. However, increasing r requires more transmitter power, which is not desirable. Hence, it appears that an optimum value of r exists, which, for a fixed total power and a given R_b/B', results in the lowest bit error rate. The next section presents the computed optimum value of r, along with the resulting error probability as a function of E_T/N_0.

III. NUMERICAL RESULTS

The bit error probability of a TCT receiver can be evaluated from Eq. (12). Since this equation cannot be solved analytically, numerical techniques were used to determine this error probability. As discussed in the previous section, for a given R_b/B', the link performance depends on the tone-to-signal power ratio r. Figure 4 shows the optimum value of r as a function of the total bit energy to noise power density ratio (E_T/N_o). This result is presented for two values of R_b/B', i.e., 20 and 50. As is apparent from this figure, the optimum r is fairly constant for medium and high values of E_T/N_o, and changes only for very low E_T/N_o. This is a very important characteristic of the single-tone TCT, since, in the presence of signal fading, the value of r does not have to be dynamically modified. In other words, one value of r is expected to provide good results over a large range of received signal power. This value of r, for example, is 0.15 for $R_b/B' = 50$.

Figure 5 illustrates the link bit error probability, again as a function of E_T/N_o and for two values of R_b/B', 20 and 50. To obtain this figure, r is optimized for each value of E_T/N_o. For $R_b/B' = 20$ and $P_e = 0.002$, the loss associated with TCT is less than 2 dB compared to ideal binary phase shift keying (BPSK).
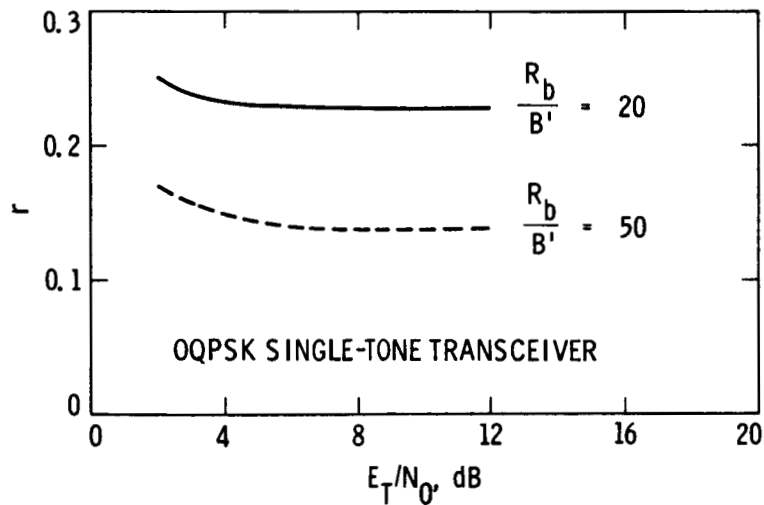
Figure 4.   Optimum value of r as a function
of E_T/N_o.
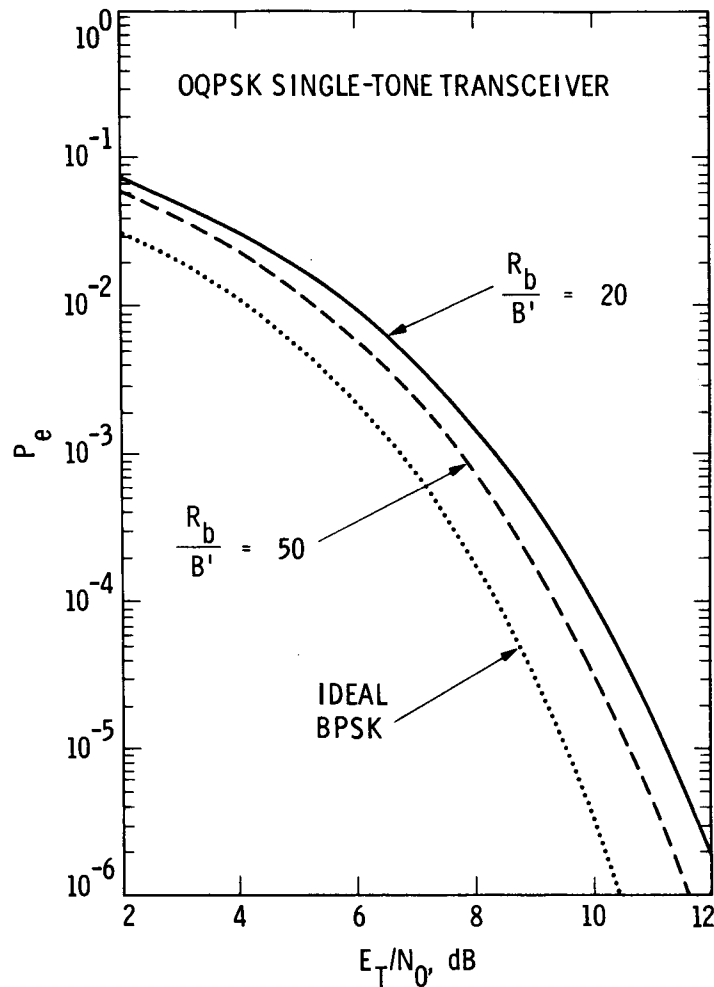
Figure 5.   Receiver error probability in the
            presence of thermal noise.

The receiver performance in the presence of Rayleigh fading is shown in Fig. 6.   Again, values 20 and 50 are used for R_b/B' with r equal to .25 and .15, respectively.   At P_e = 0.002, this receiver performs about 2 dB worse than the ideal BPSK in the presence of fading.   Note that in the 800-MHz band (Doppler close to 100 Hz) when R_b = 2400 bps, this error probability, P_e = 0.002, is well below the error floor of all the conventional receivers, including FM (Ref. 14), coherent BPSK, and differentially coherent BPSK. Finally, Fig. 7 demonstrates the result for a Rician fading channel for K = 10.   This value of K is concluded from the experiments conducted recently as a conservative estimate of the satellite-aided mobile link characteristic. Such empirical studies performed by the National Aeronautics and Space Administration (NASA) are aimed at modeling and verifying the propagation environment of mobile links using satellite repeaters.
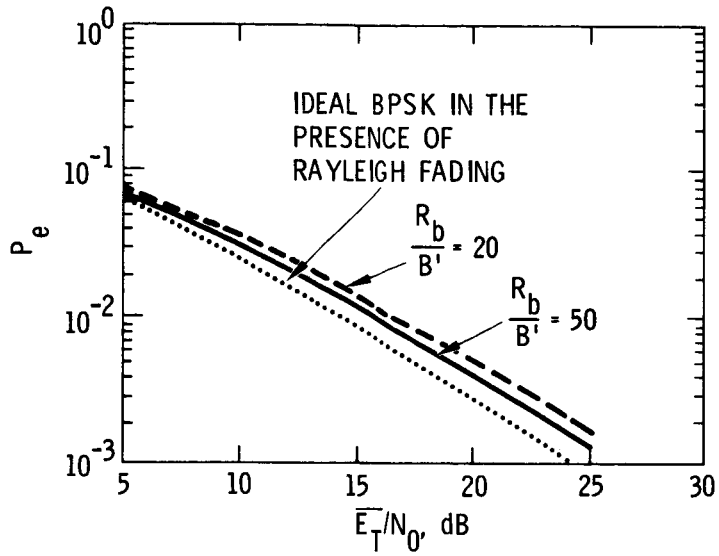
Figure 6.   Receiver performance in the presence
of Rayleigh fading.
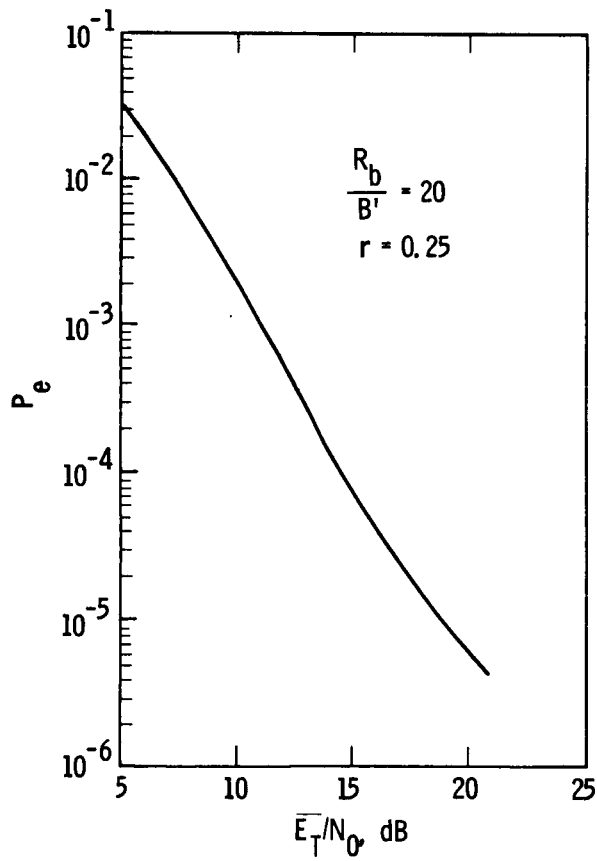
Figure 7.   Receiver performance in the
presence of Rician fading,
$K = 10$.

IV. RECEIVER IMPLEMENTATION AT BASEBAND

The TCT receiver proposed in the previous sections poses certain practical difficulties in view of the stringent phase and amplitude response requirements of the pilot bandpass filter (PBPF). Construction of very narrow filters at a reasonable IF frequency such as 45 MHz is very difficult. Hence, the two attempts at verifying the TCT concept by the General Electric Company (Ref. 15) and Motorola (Ref. 16) were performed at the very low IF frequency of 10 kHz. To avoid the obstacles associated with the construction of the modem at IF, baseband fabrication of the receiver appears advantageous.

The baseband TCT receiver, which is equivalent in its outcome to the one shown in Fig. 2, is illustrated in Fig. 8, where both in-phase and quadrature components have now been considered. This scheme has the advantage of using baseband components instead of RF components. With this configuration, the received waveform is first transformed to baseband by in-phase and quadrature noncoherent multipliers. Next, two pilot lowpass filters (PLPF) are used to select the two components of the pilot tone. Note that the noncoherent demodulation operations have transformed the pilot tone into a pair of in-phase and quadrature slowly varying waveforms at points u_i and u_q.

The calibration subsystem, which is an amplitude normalizer, has a simple structure at baseband. This function is identified by the dashed line in Fig. 8. Note that the waveforms at points v_i and v_q have an amplitude proportional to the inverse of the pilot tone amplitude.

The noise analysis of the baseband receiver is similar to that of the IF. Indeed, one can show that the two receivers are equivalent.* To demonstrate this, we may, in a way similar to the previous case, decompose the white noise into two disjoint components: one that falls within the bandwidth of PLPF, and one that does not. Note that PLPF filters are lowpass equivalents of PBPF in Fig. 2. Hence, the bandwidth of PLPF is $B'/2$. Since Eq. (3) describes the sum of the pilot and the former noise term at IF, at baseband (output of PLPF) this signal is represented by the following:

$$U_i(t) = \rho \cos [Y_t + \Theta(t)]$$

$$U_q(t) = - \rho \sin [Y_t + \Theta(t)]$$

(14)

where the double frequency terms are omitted. Note that we may write

$$\rho^2 = U_i^2(t) + U_q^2(t)$$

(15)

---

*This was done by Marvin Simon of JPL. The following analysis is largely due to his efforts.
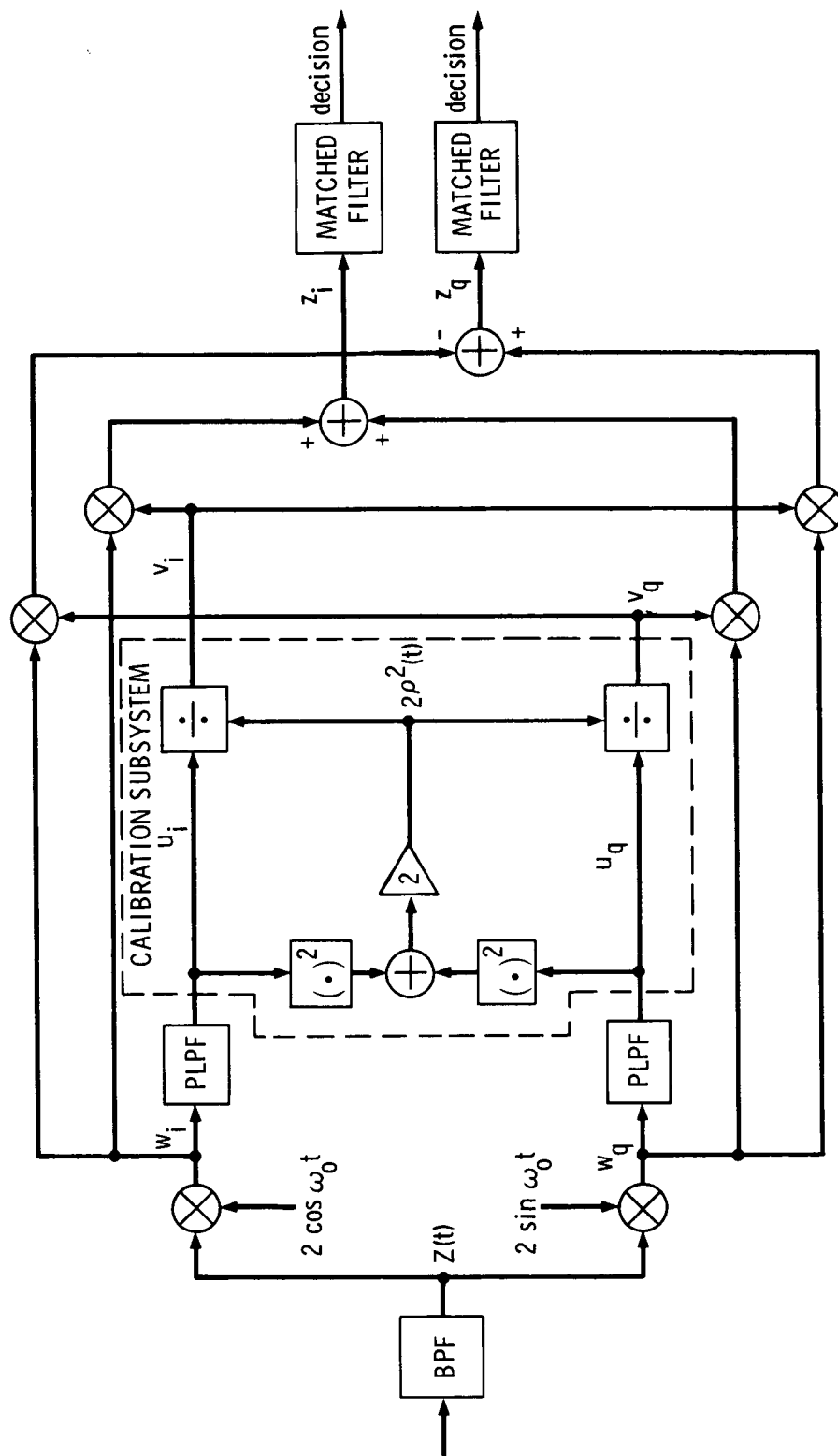
Figure 8. Baseband equivalent of Fig. 2 including in-phase and quadrature components.

The signals at points w_i and w_q (input to PLPF) are composed of the data-bearing signal, the pilot, and the two spectrally disjoint noise terms. Therefore

$$W_i(t) = U_i(t) + S_1(t) + \tilde{N}_i(t)$$

$$W_q(t) = U_q(t) + S_2(t) + \tilde{N}_q(t)$$

(16)

where $\tilde{N}_i(t)$ and $\tilde{N}_q(t)$ are white Gaussian noise processes defined earlier in Eq. (6). Furthermore, $S_1(t)$ and $S_2(t)$ are given by

$$S_1(t) = \frac{A}{\sqrt{2}} X_t \{S_i(t) \cos(Y_t) + S_q(t) \sin(Y_t)\}$$

(17)

$$S_2(t) = \frac{A}{\sqrt{2}} X_t \{-S_i(t) \sin(Y_t) + S_q(t) \cos(Y_t)\}$$

At points z_i and z_q the signals can be expressed by the following terms:

$$Z_i(t) = \frac{1}{2\rho^2} [W_i(t)U_i(t) + W_q(t)U_q(t)]$$

(18)

$$Z_q(t) = \frac{1}{2\rho^2} [-W_i(t)U_q(t) + W_q(t)U_i(t)]$$

or

$$Z_i(t) = \frac{1}{2\rho^2} [U_i^2(t) + U_q^2(t)] + \frac{1}{2\rho^2} [S_1(t)U_i(t) + S_2(t)U_q(t)]$$

$$+ \frac{1}{2\rho^2} [\tilde{N}_i(t)U_i(t) + \tilde{N}_q(t)U_q(t)]$$

$$Z_q(t) = \frac{1}{2\rho^2} [-S_1(t)U_q(t) + S_2(t)U_i(t)] + \frac{1}{2\rho^2} [-\tilde{N}_i(t)U_q(t) + \tilde{N}_q(t)U_i(t)]$$

Substituting Eqs. (6), (14), and (17) into the above equations and ignoring the double frequency terms bring about the following final result:

$$Z_i(t) = \frac{1}{2} + \frac{AX_t}{2\sqrt{2}\rho(t)} \{S_i(t) \cos[\theta(t)] - S_q(t) \sin[\theta(t)]\} + \frac{1}{2\rho(t)} \tilde{N}(t)$$

$$\text{(19)}$$

$$Z_q(t) = \frac{AX_t}{2\sqrt{2}\rho(t)} \{S_q(t) \cos[\theta(t)] + S_i(t) \sin[\theta(t)]\} + \frac{1}{2\rho(t)} \tilde{N}(t)$$

Note that the above equation for $Z_i(t)$ is identical to Eq. (5). Therefore, it is established that the representation of Fig. 8 is equivalent to that of Fig. 2. Hence the numerical results of Figs. 4 through 7 are also valid for the receiver implementation at baseband. In Eq. (19) $\tilde{N}(t)$ is given by

$$\tilde{N}(t) = \tilde{N}_i(t) \sin[Y_t + \theta(t)] + \tilde{N}_q(t) \cos[Y_t + \theta(t)] \tag{20}$$

V. REMARKS

The analysis of a TCT receiver in the presence of thermal noise and fading, ignoring certain hardware imperfections, has been presented. There are two areas of concern for realization of the TCT scheme: creation of a pure spectral null at the transmit end, and delay matching of the different paths at the receiver end. The former impediment can be removed by taking advantage of digital signal processing techniques. The precise signal spectral shape can be achieved by digital processing of channel pulses. Both the Nyquist and the highpass filters of Fig. 1 can be incorporated in a digital algorithm, as will be discussed in the next section. This algorithm can also include encoding and other necessary functions. Nevertheless, an analysis that includes the effects of self-interference can be useful. Although the TCT approach is insensitive to Doppler and small frequency errors, its performance is expected to severely degrade in the presence of a large frequency offset. A further analysis of this technique should also include the effects of a frequency error on the receiver performance. In practice, the potential frequency uncertainty will be minimized by employing some form of automatic frequency control (AFC).

The spectral property of the TCT signal can be improved by utilizing more efficient means of spectral shaping than the Manchester code. Spectrum parting (Ref. 6) and balanced encoding (see the appendix) are good alternatives to the Manchester code that result in smaller spectral occupancy. Figure 9 shows the power spectral density of the OQPSK signal with Manchester encoding when Nyquist pulses are used. The bandwidth-time product (BT) of this signal is unity.

To fully exploit the TCT benefits (power and spectrum), the resulting signal ends up being of the nonconstant envelope type. This may be considered a drawback for this technique because the mobile terminals must use more expensive linear amplifiers to accommodate the nonconstant amplitude of the carrier. However, this is not a severe problem, since amplifier technology is rapidly improving. Particularly with the recent interest in amplitude compandored single-sideband (ACSB) transmission of voice over mobile channels, it is expected that low-cost linear power amplifiers will soon become commercially available.
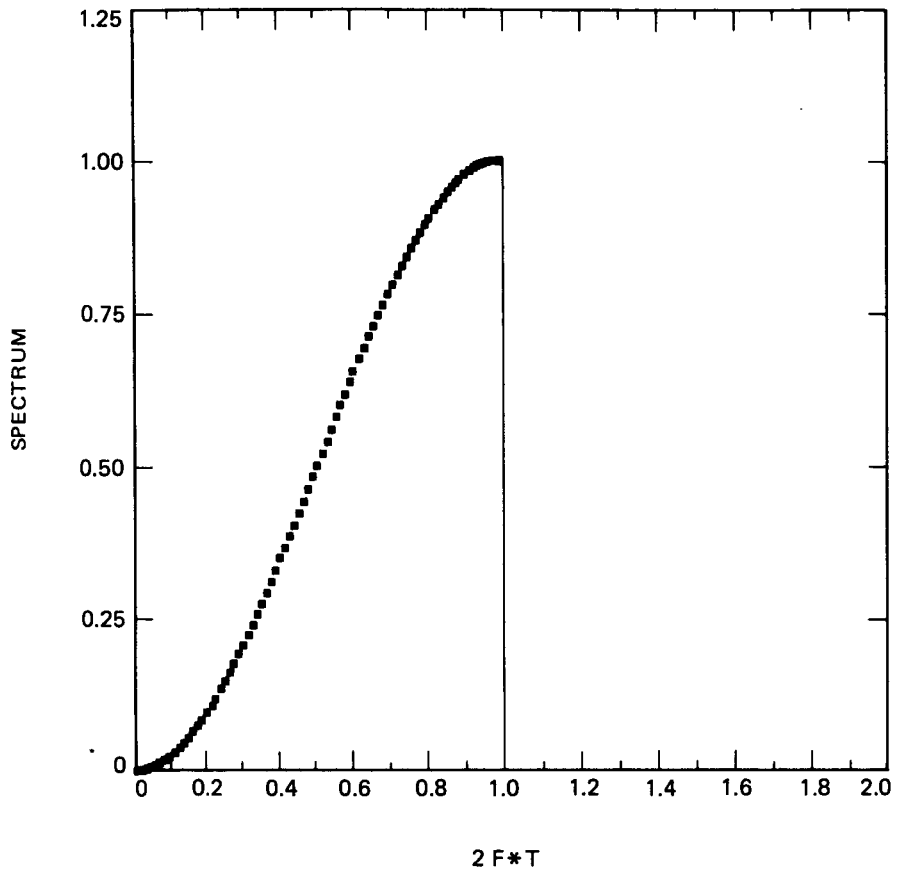
Figure 9. Power spectral density of Manchester coded waveform.

VI. BREADBOARDING OF THE TRANSMITTER

Construction of a TCT transmitter is an exacting process. Because of the critical role the pilot plays in signal demodulation, it has to be well protected from interference. Furthermore, signal distortions created by spectral nulling must be minimized. Hence, the TCT transmitter must be implemented with extreme precision. This section describes a generic technique that yields a transmitter having flexibility and precision. This approach uses digital components and can be used for generation of a wide variety of signals.

A. MODULATOR FORMULATION

A broad class of digital modulation techniques can be formulated by a common equation (Ref. 17). The equation that symbolizes the carrier modulation has a quadrature form and is given below:

$$c(t) = a(t) \cos \omega_c t + b(t) \sin \omega_c t \tag{21}$$

In the above equation c(t) denotes the resulting modulation at carrier angular frequency of ω_c, and a(t) and b(t) denote two baseband information-bearing signals. Equation (21) can represent common modulation schemes such as frequency shift keying (FSK), BPSK, QPSK, M-ary Phase Shift Keying (MPSK), quadrature amplitude modulation (QAM), etc. Waveforms a(t) and b(t) assume a different form for each modulation scheme. Table 1 presents an example wherein waveforms a(t) and b(t) are defined.

Equation (21) can also be used when modulation is bandlimited and intersymbol interference (ISI) exists. The simple form of Eq. (21) suggests that a single circuit can be used to generate a broad class of modulation techniques. A simple approach is described that uses digital signal generation techniques to implement Eq. (21).

Signal bandlimiting at the transmitter can be performed either at baseband, before modulation, or at radio frequency (RF), after modulation. Most spectrum conservation techniques can be represented by one of the diagrams shown in Fig. 10. Diagram A in Fig. 10 uses a filter after modulation; whereas, diagram B uses a filter before modulation. Diagrams A and B are equivalent and usually result in a nonconstant envelope carrier. Diagram C uses a nonlinearity after the filter (before modulation). This approach is usually used if a constant envelope signal is desired (Ref. 18). Although the technique described in this report is also suitable for signals generated by Diagram C, for brevity, only signals generated by Diagram B will be discussed here.

TABLE 1. Modulation Examples

Modulation	Description
BPSK	$b(t) = 0$.
QPSK	$a(t)$ and $b(t)$ are independent.
MPSK	$a(t)$ and $b(t)$ are dependent.
Binary FM	$a(t) = \cos \Delta\omega t$; $b(t) = m(t) \sin \Delta\omega t$; $\Delta\omega$ is the frequency deviation; and $m(t)$ is the NRZ encoded source output.
SSB	$b(t)$ equals the Hilbert transform of $a(t)$.
QAM	$a(t)$ and $b(t)$ may be dependent.

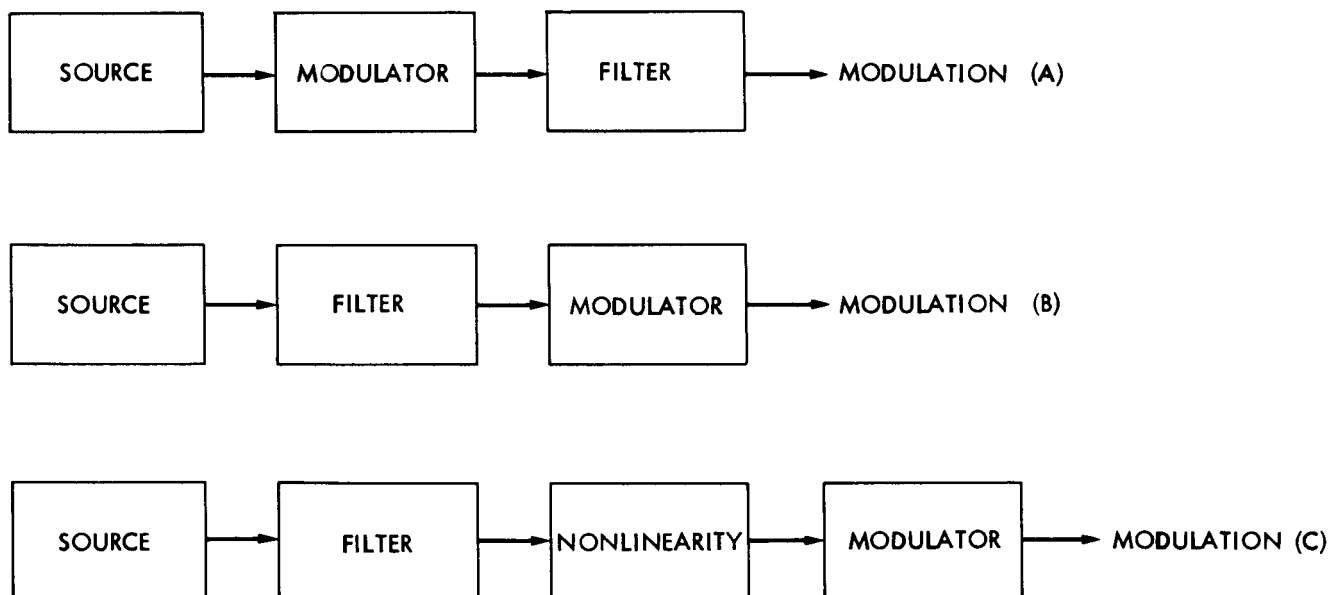NRZ: Not return to zero
SSB: single sideband

Figure 10. Different methods of signal filtering.

B. GENERATION OF SIGNAL CONSTELLATION

The signal constellation can be viewed as a two-dimensional structure. Each point on the constellation can be defined by a pair of coordinates on the X-Y axes. It is convenient to select a pair of orthogonal coordinate axes. If these axes are represented by $\cos \omega_c t$ and $\sin \omega_c t$, the coordinates are functions $a(t)$ and $b(t)$ of Eq. (21). For some signal constellations $a(t)$ and $b(t)$ are independent random functions; while for others, they are not independent. Whether $a(t)$ and $b(t)$ are statistically independent or not, they are processed (i.e., filtered) independently.

As an example, the waveform constellation for a nonuniform 8-PSK signal is shown in Fig. 11. Nonuniform structures have been shown to be an advantage for certain applications (Ref. 19). For the signal constellation of Fig. 11, the coordinate functions $a(t)$ and $b(t)$ are quaternary waveforms assuming values proportional to $\pm \cos \theta$ and $\pm \sin \theta$, where θ is an angle that determines the constellation shape $(0 \leq \theta \leq \pi/2)$. For $\theta = \pi/4$, the constellation becomes uniform. For this example (8-PSK), the binary source output is sampled three bits at a time. Each sample assumes one of the eight known states or positions on the circle shown in Fig. 11. For example, the coordinates associated with the source output (000) are $a(t) = \cos \theta$ and
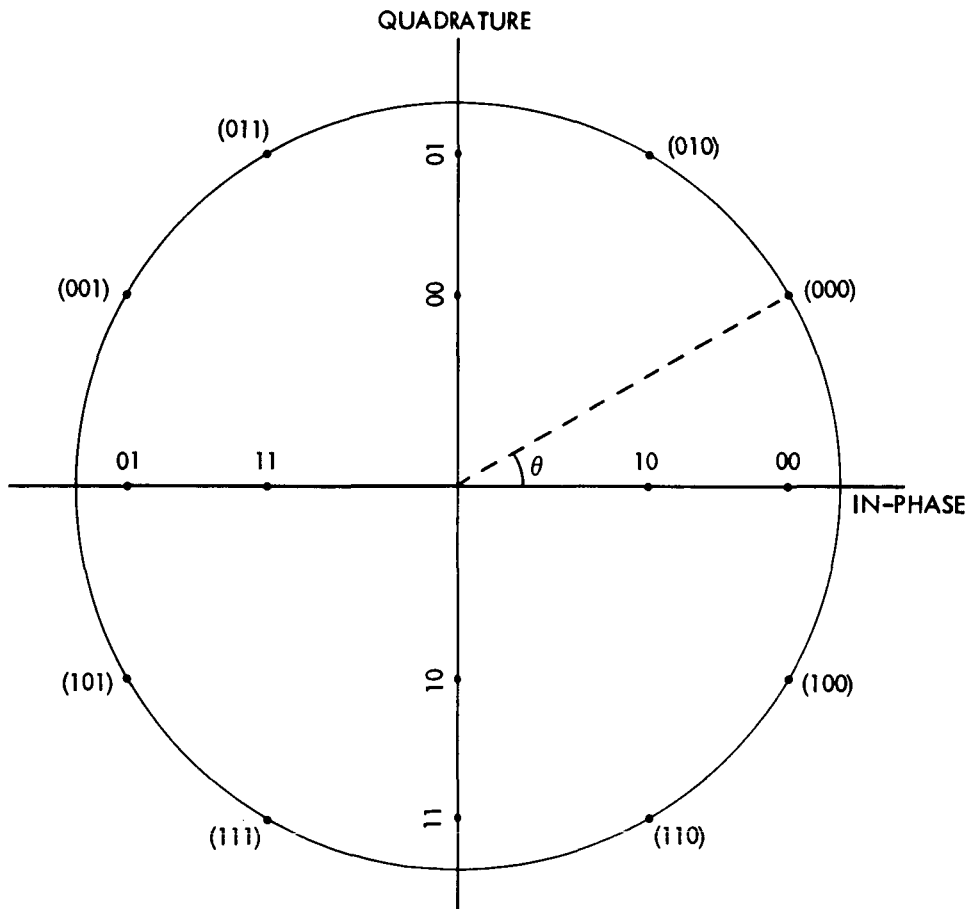

Figure 11. A nonuniform signal constellation.

$b(t) = \sin \theta$. As mentioned previously, for an 8-PSK system, the source output is sampled three bits at a time. The two most significant bits are used to define the X coordinate, $a(t)$, and the two least significant bits are used to define the Y coordinate, $b(t)$. Because the middle bit is shared between $a(t)$ and $b(t)$, these two waveforms are correlated. Table 2 tabulates the potential values of $a(t)$ and $b(t)$ as α_i and β_i (see Eq. (22)) for this example.

Table 2. Coordinate Functions of Nonuniform 8-PSK Signal

Two-Bit State	α_i	β_i
00	$\cos \theta$	$\sin \theta$
01	$-\cos \theta$	$\cos \theta$
10	$\sin \theta$	$-\sin \theta$
11	$-\sin \theta$	$-\cos \theta$

C. SIGNALING PULSE SHAPE

Signaling pulse shape influences the carrier spectrum. Pulse shaping is achieved by filtering. Although, in general, $a(t)$ and $b(t)$ are correlated, they can be filtered separately. Letting $h(t)$ denote the pulse shape, waveforms $a(t)$ and $b(t)$ can be formulated as

$$a(t) = \sum_i \alpha_i h(t - iT)$$

$$b(t) = \sum_i \beta_i h(t - iT)$$

(22)

where α_i and β_i depend on the source output at time iT. (For 8-PSK, see Table 2.) T denotes the symbol duration, and i denotes a symbol count index. For an 8-PSK signal, for example, symbol duration T is three times the source bit duration. In the absence of band limitation, $h(t)$ is confined to a symbol time, hence, avoiding ISI. In the presence of bandwidth limitation, $a(t)$ and $b(t)$ are affected by more than one symbol.

Since $a(t)$ and $b(t)$ are bandlimited in practice, they may be sampled using an adequate sampling rate. Let τ denote the sampling period. The samples of $a(t)$ and $b(t)$ at symbol duration n are written as

$$a(nT + j\tau) = \sum_i \alpha_i h[j\tau + (n - i)T]$$

$$\text{(23)}$$

$$b(nT + jt) = \sum_i \beta_i h[j\tau + (n - i)T]$$

where j is an integer pointing to the sample position within a symbol duration. Assuming L samples per symbol are taken, $1 \leq j \leq L$. In practice ISI is limited to a finite number of symbols. Let the ISI length in terms of symbols be 2M. Hence

$$a(nT + j\tau) = \sum_{k=-M}^{M-1} \alpha_{-k+n} h(j\tau + kT) \qquad \text{(24-a)}$$

$$b(nT + j\tau) = \sum_{k=-M}^{M-1} \beta_{-k+n} h(j\tau + kT) \qquad \text{(24-b)}$$

Equations (24-a) and (24-b) indicate that each sample of a(t) and b(t) results from 2M multiplications. Clearly 2ML multiplications per symbol are required to generate a(t), and similarly, 2ML multiplications per symbol are required to generate b(t). Hence, the total number of multiplications per second required to generate samples of a(t) and b(t) is 4ML/T. Parameters M, L, and the quantization resolution must be selected such that distortions resulting from truncation, sampling, and quantization remain small (Ref. 18).

D.   MODEM ARCHITECTURE

Figure 12 shows the modulator architecture. The source output is fed into a circuit that determines the coefficients α and β. The input clock to this box has frequency 1/T. The outputs of this circuit are sampled 1/T per second. The values of α_n and β_n are used independently in two identical arms of Fig. 12. The sample generators provide the samples of a(t) and b(t). The samples are converted into two analog signals by the digital to analog convertors (DAC) and modulate the carrier in a quadrature modulator, resulting in c(t). The clock frequency of the sample generator is 1/τ. The sample generator is the heart of the modulator in Fig. 12. It is of prime importance to implement the sample generator in a generalized fashion to ensure that the same circuit can be used for a broad class of modulation techniques.

Figure 13 shows the block diagram of the sample generator. Because the two sample generators function similarly, only the upper arm is described here. The sample generator consists of a shift register with 2M stages to keep the most recent 2M values of α_n and a memory with 2M banks to store the pulse shape. Each bank of this memory consists of L words where each word stores a sample of the pulse shape. The word size depends on the quantizer
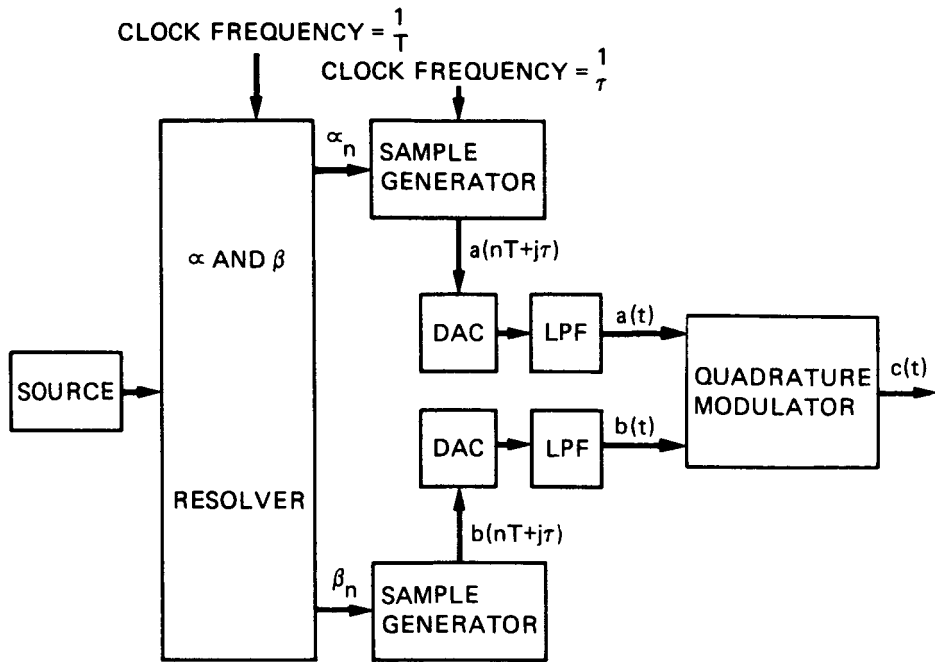
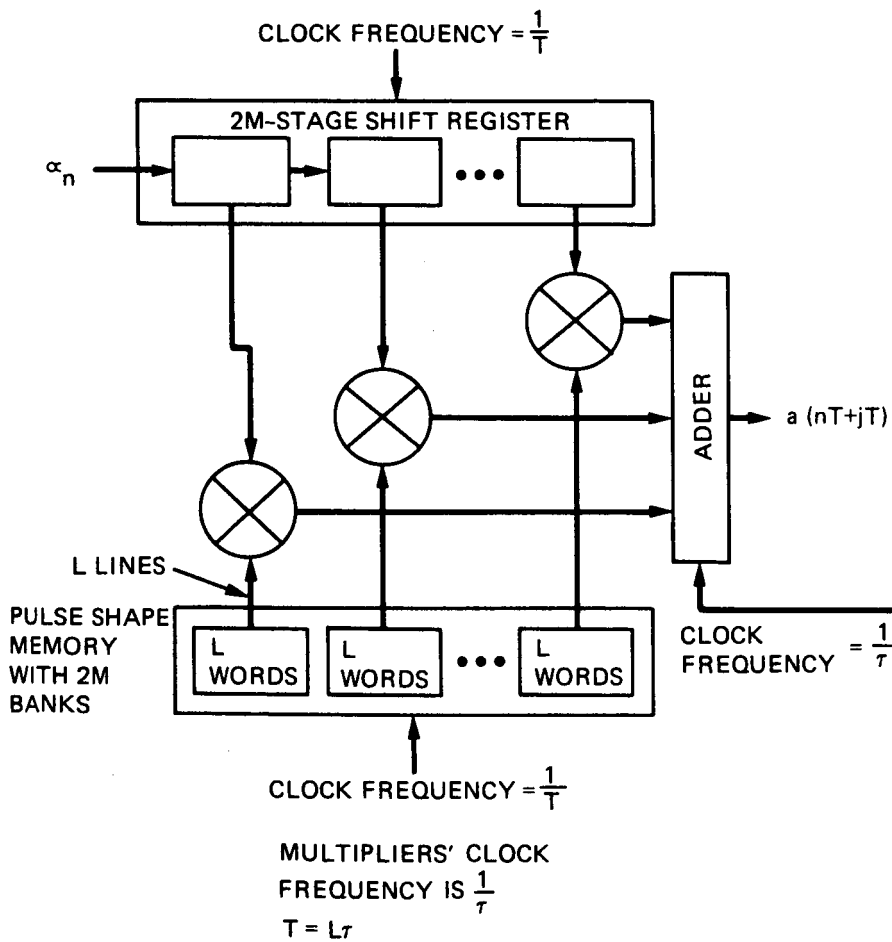Figure 12. Generalized block diagram of modulator hardware.

Figure 13. Sample generator architecture.

resolution. The shift register is clocked with 1/T frequency; whereas, the pulse-shape memory is clocked with 1/τ frequency. Note that T/τ = L. The multipliers are operated 1/τ per second to implement the product operation in Eq. (24-a). The summer adds the 2M inputs to produce a sample of a(t).

Because the required multiplication rate is relatively slow for most applications, Fig. 13 can be modified to use only one multiplier instead of 2M. Figure 14 shows the sample generator with serial multiplication rather than parallel. This method results in a great component saving with slight added implementation complexity. Note that in the present configuration the stored data in the memory banks have been rearranged and now there are L banks (instead of 2M) with each bank containing 2M samples.
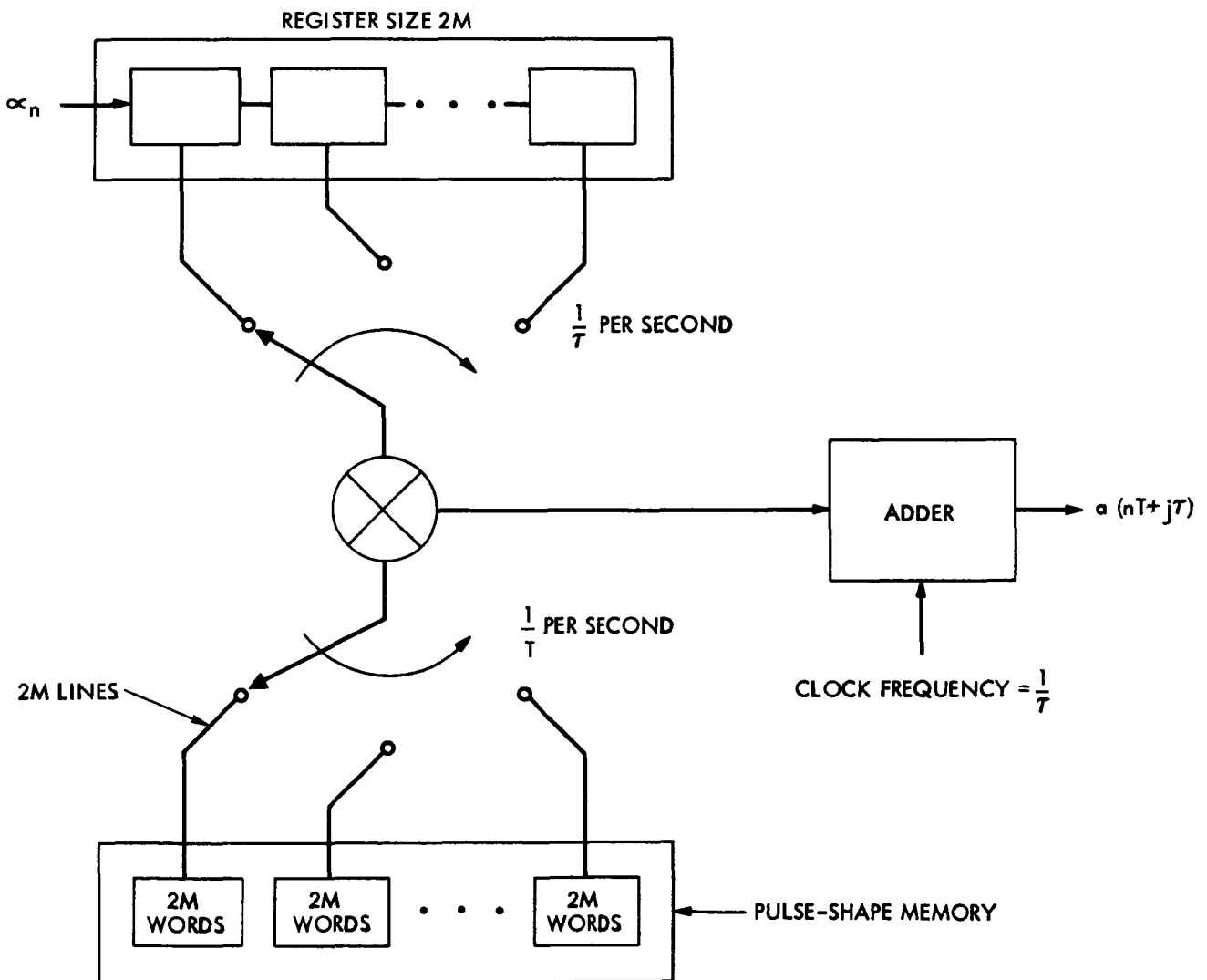

Figure 14. Modified architecture for the sample generator using one multiplier instead of 2M.

Since ISI length is 2M and pulse shape h(t) is presented by L samples per symbol, the total number of samples is 2ML with each memory bank containing 2M samples. Let the samples of h(t) be denoted by h_i where $1 \leq i \leq 2ML$. In Fig. 14, data are stored in memory as follows: The first bank contains samples for i = 1, L + 1, 2L + 1, .., (2M - 1) L + 1; the second bank contains samples for i = 2, L + 2, 2L + 2, .., (2M - 1)L + 2; the last bank contains samples for i = L, 2L, .., 2ML. The values stored temporarily in the shift register are multiplied by the content of the first memory bank serially in a time-shared fashion and added in the adder. The cycle repeats for the second memory bank, and continues until the contents of all the banks have been accessed. At this point, a new value enters the shift register, pushing the content of the registers one stage to the right and dropping off the oldest datum. Then the previously noted cycles repeat. The multiplier rate with this configuration is 2ML/T multiplications per second.

The modulator of Fig. 13 or 14 is very versatile. The pulse shape or the spectral shape of the carrier can be changed by simply changing the contents of the memory banks. Similarly, any source bit rate can be accommodated by simply changing the clock rate. Simple modification of the memory banks in the sample generator and the coefficient resolver of Fig. 12 could result in a different modulation scheme. For example, this modulator can change from an FM system to an SSB-AM system by the flip of a switch.

Figure 15 shows the transmitter prototype used to conduct the experiments described in the following section. This transmitter can be greatly reduced in size using off-the-shelf components. For example, the shift register boards can easily be replaced by a pair of random access memory (RAM) chips. Using off-the-shelf components, the transmitter can be fabricated on a single board. Employing Very Large Scale Integration (VLSI) techniques, the transmitter can be reduced to a small fraction of a board.

E. EXPERIMENTAL RESULTS

The TCT transmitter shown in Fig. 1 was developed using the prototype transmitter of Fig. 15. The objective here is to create a deep null in the data spectrum to transmit a tone (residual carrier) along with the modulation. The proposed method to create this spectral null is to combine Manchester encoding and highpass filtering. To protect the tone from self-interference, the spectral null must be clean. Furthermore, the null width is carefully selected to allow tone detection in spite of Doppler shift and a small frequency error. It is required that filtering, particularly the highpass, must be performed without added distortion. Poor filtering operation results in "severe eye closure" and increased out-of-band power. To maintain utmost signal integrity, the signal spectrum design was conducted on a computer (a Digital Equipment Corporation VAX was used). The signal design included a raised-cosine filter with a roll-off factor of 0.5. Because a(t) and b(t) are statistically independent processes for QPSK, the coefficient resolver circuit allocates odd source bits to α_n and even bits to β_n. The source bit rate is 2400 bps with T = 1/1200. The combined effect of Manchester encoding, highpass filtering, and raised-cosine pulse shaping is a signal spectrum shown in Fig. 16, which shows the Fourier transform of a pulse as a function of frequency. The signal band occupancy is 1800 Hz. The spectral null width is about 100 Hz at -40 dB.
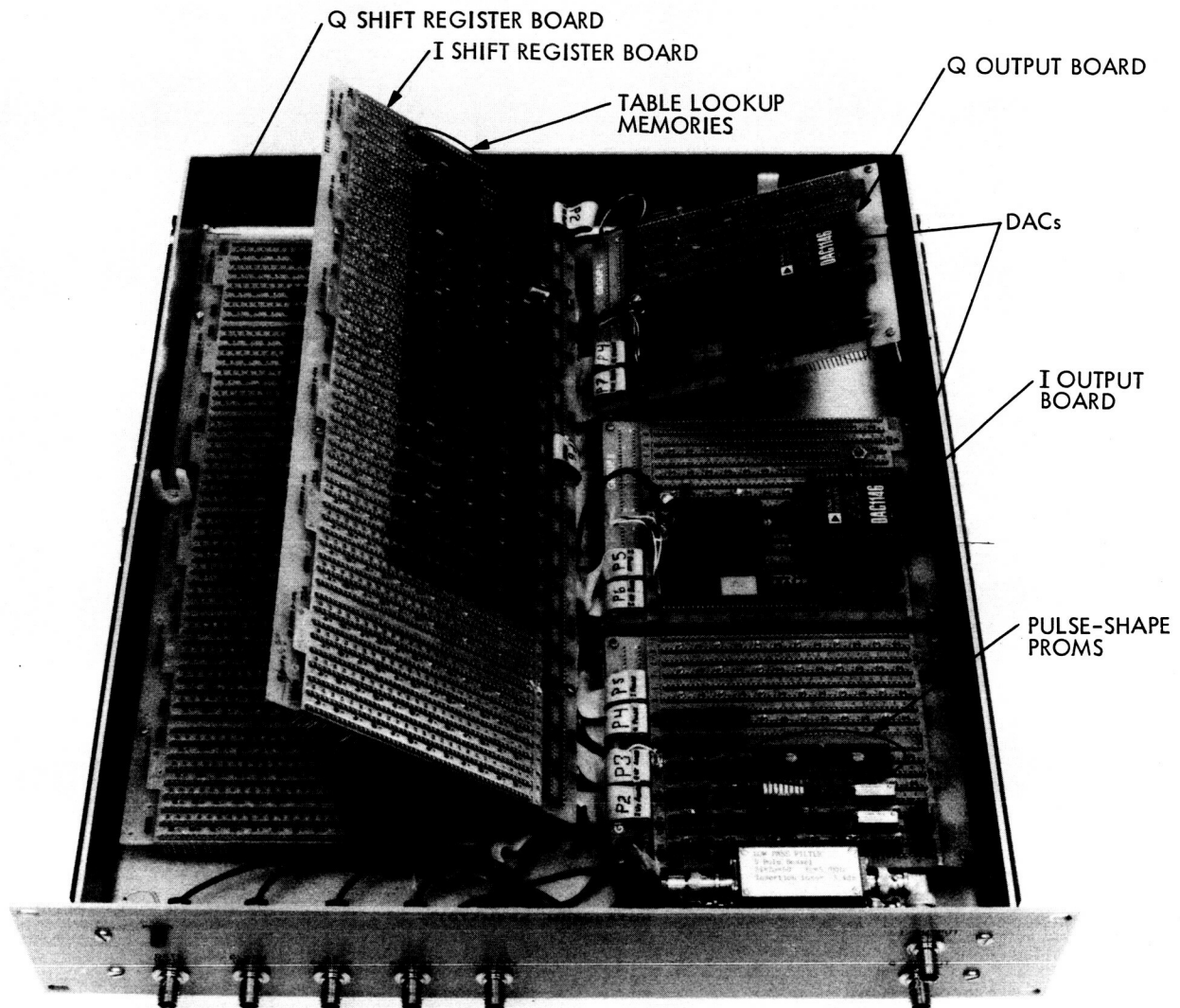
Figure 15. Multipurpose all-digital transmitter prototype.
Using off-the-shelf components, the transmitter can
easily be implemented on a single board.

Figure 17 shows the time domain pulse (inverse Fourier transform of
Fig. 16). From Fig. 17, it is evident that pulse spreading is about
18 symbols, hence M = 9. Because the signal bandwidth is 1800 Hz, Nyquist's
theorem requires a sampling frequency of 3600 Hz. This means that at least
three samples per symbol must be taken to avoid aliasing. For practical
considerations and ease of implementation of the lowpass filters in Fig. 13,
sampling is performed with four times the minimum required rate, i.e.,
12 samples per symbol. Therefore, L = 12. The total number of samples
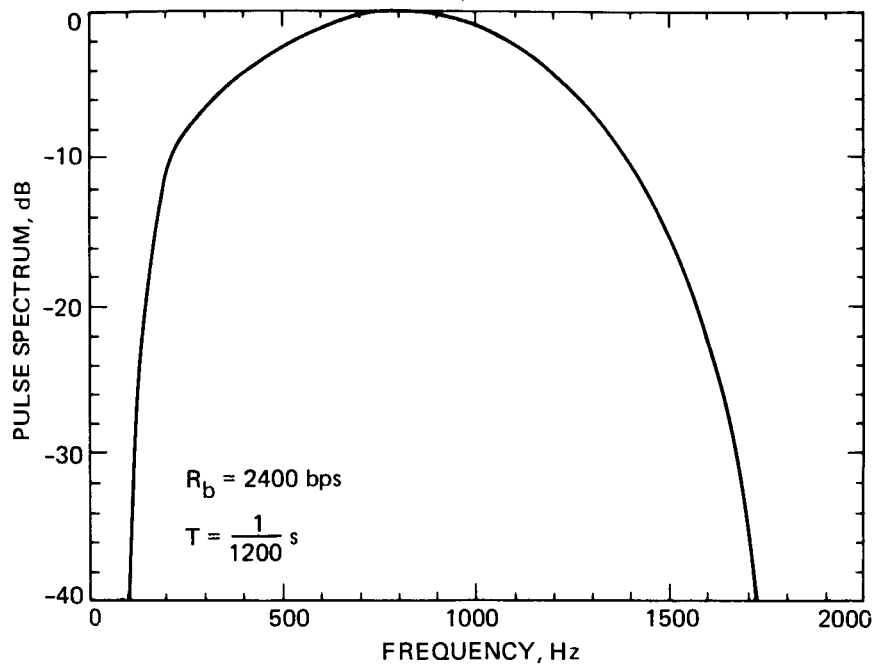
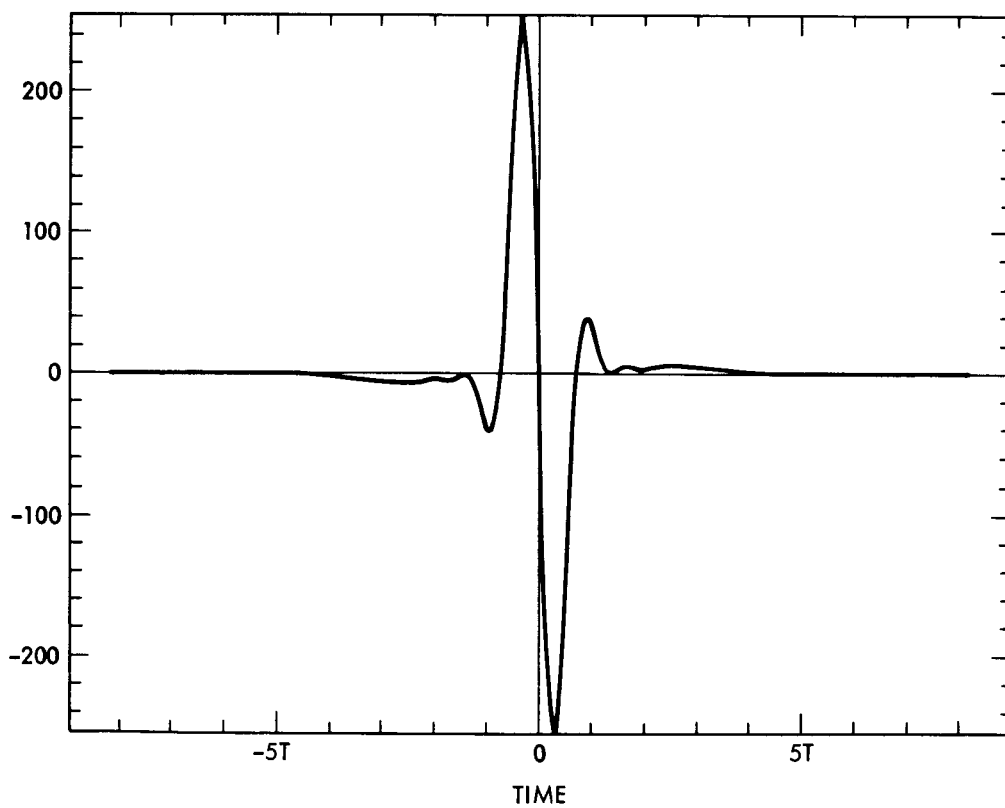Figure 16. Spectrum of the signaling pulse in a TCT/QPSK modulator.

Figure 17. Pulse function obtained by inverse Fourier transforming of the spectrum of Fig. 16 on a digital computer.

representing the pulse shape is 2LM or 216. A nine-bit quantizer is used to convert the sample values into binary quantities. Parameters L, M, and the quantizer's resolution are selected conservatively to avoid potential distortion.

Figure 18 shows waveform a(t) at the output of the DAC (see Fig. 12) when the source output is all ones; the DAC resolution is 16 bits. Figure 19 shows the eye pattern when data are randomized. Figure 20 shows the signal spectrum. In Fig. 20 the spectral sidebands are 14.4 kHz apart; sideband attenuation due to "sample and hold" is evident. The lowpass filter(s) in Fig. 12 removes the high frequency harmonics, resulting in a smoothed output. The filter output is described in Figs. 21 to 23. Figure 21 shows the
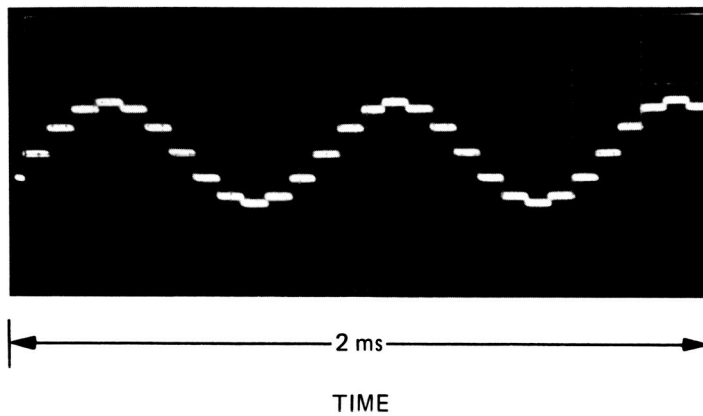

|←————————— 2 ms —————————→|

TIME

Figure 18. All-ones waveform.

|←————————— 2 ms —————————→|

TIME
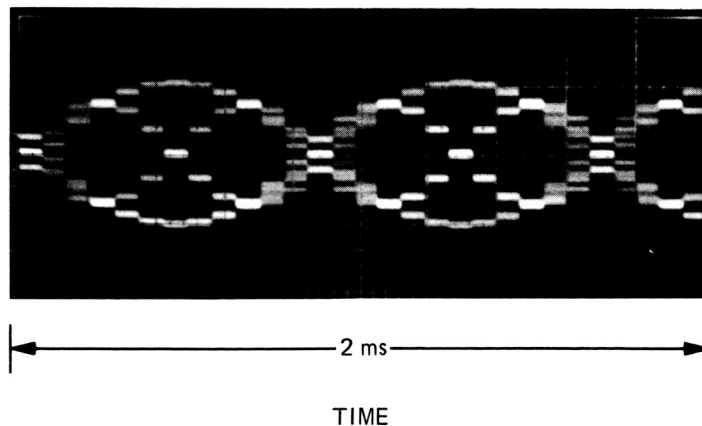
Figure 19. Eye pattern.

all-ones waveform. Figure 22 shows the eye pattern. Figure 23 shows the power spectrum of the signal, which looks like the one generated numerically (see Fig. 16). Figure 24 shows the sample power spectrum with expanded frequency scale. Here the spectral null can be seen closely. It is evident that this null is clear of self-interference. Figure 25 shows the signal spectrum at the output of the quadrature modulator. A pilot tone, 6 dB below the signal in power, is added to the carrier in Fig. 25.

├──────────100 kHz──────────────►┤

FREQUENCY
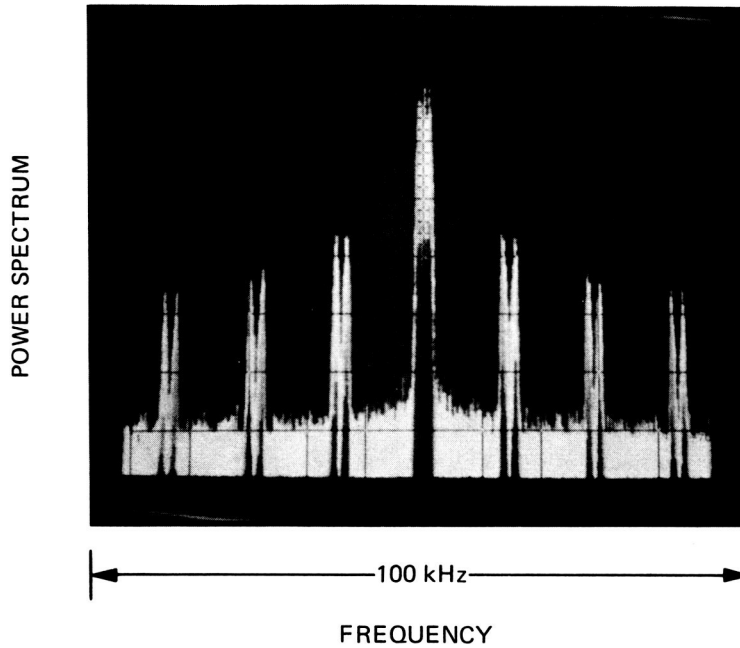
VERTICAL SCALE: 10 dB/div

Figure 20. Signal spectrum.

├──────────────2 ms──────────────►┤

TIME
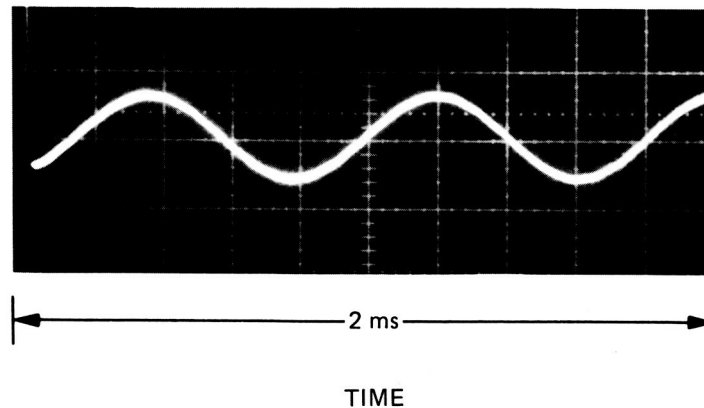
Figure 21. All-ones waveform after removal
of the sampling harmonics.

|← 2 ms →|

TIME
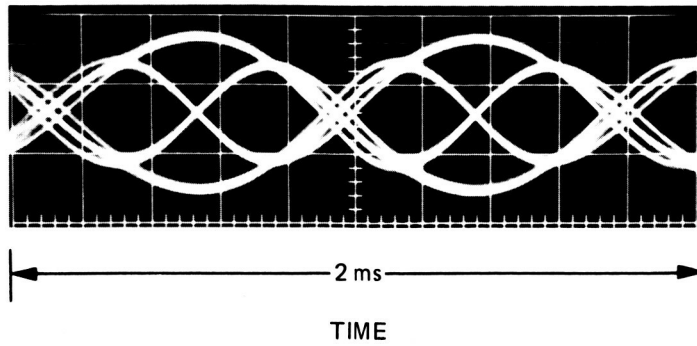
Figure 22. Eye pattern after removal of the
sampling harmonics.

|← 5 kHz →|

FREQUENCY

VERTICAL SCALE: 10 dB/div

BIT RATE: 2400 bps
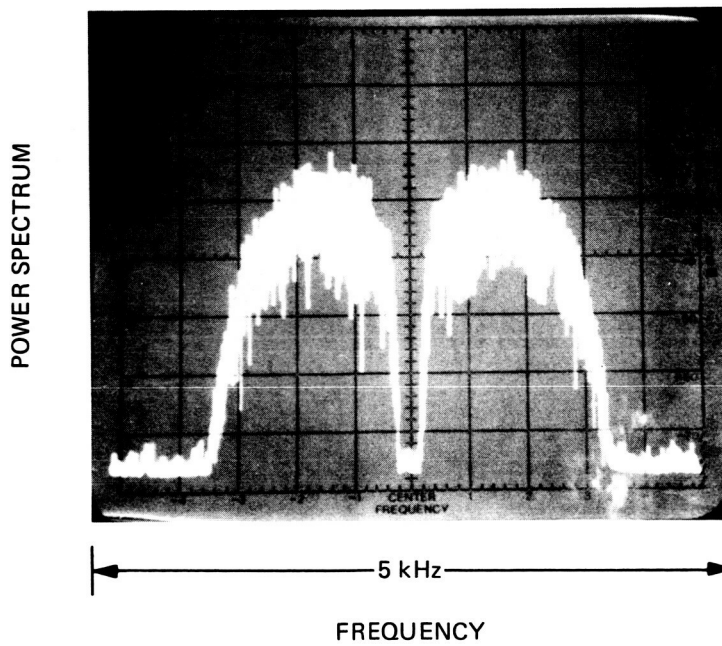
Figure 23. Measured signal spectrum
for TCT/QPSK.
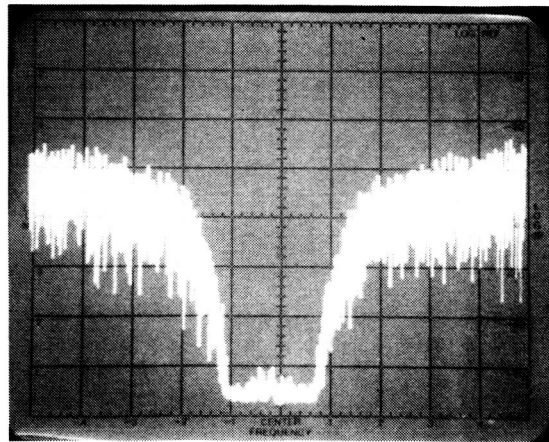
——————— 1000 Hz ———————

FREQUENCY

VERTICAL SCALE: 10 dB/div

Figure 24.   Expanded spectral null.

——————— 1000 Hz ———————

FREQUENCY

VERTICAL SCALE: 10 dB/div

Figure 25.   Signal spectrum with a
tone added.

In another instance, the transmitter memory was reprogrammed to generate a conventional QPSK signal using raised-cosine spectral shaping with a roll-off factor of 1. This particular pulse shape is spectrally very efficient without suffering from ISI. Figure 26-a shows the signal spectrum, and Fig. 26-b shows the pulse function in the time domain. The waveform of Fig. 26-b was sampled at a rate of 12 samples per symbol time (symbol rate is 1200 symbols/s) and was quantized using a nine-bit quantizer. The waveform was truncated to ± 3 symbols (M = 3). The sampled values were stored in the transmitter memory.
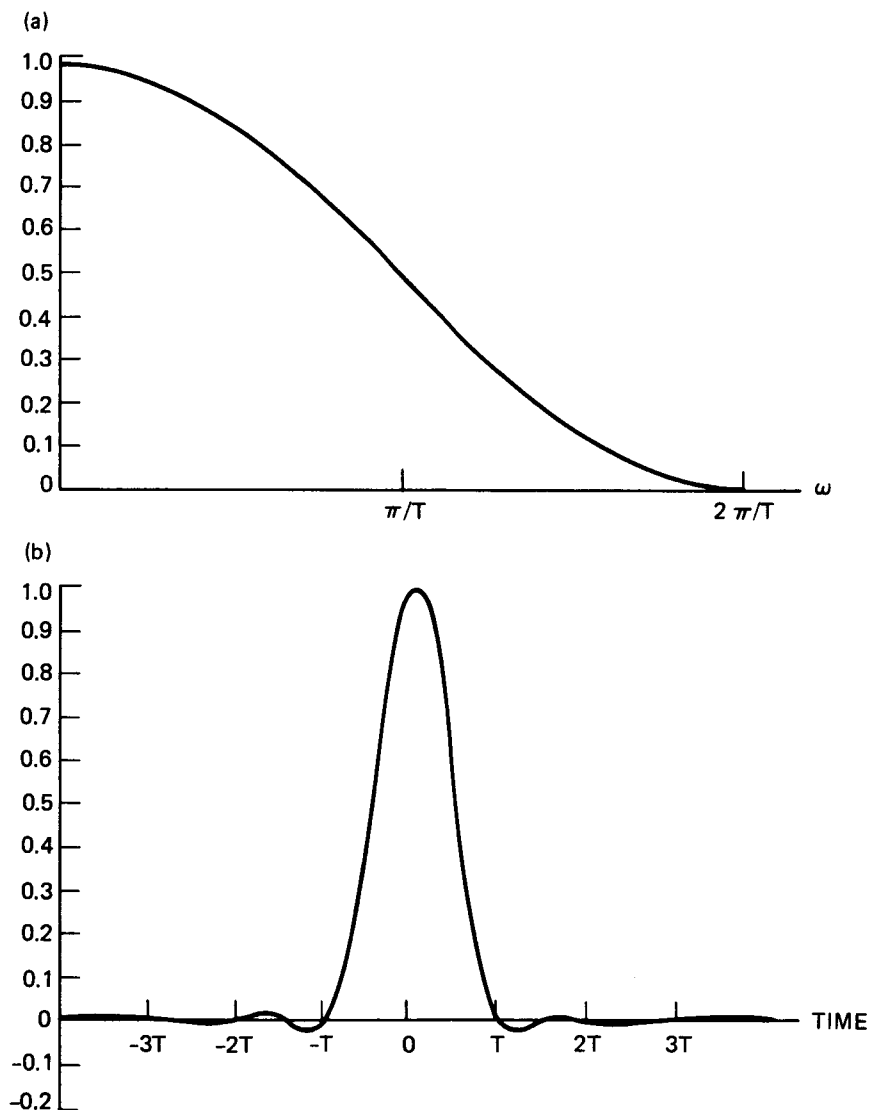

Figure 26. Raised-cosine shaping. (a) Frequency response. (b) Time response.

Figures 27 and 28 show the recorded spectrum and the eye pattern of the signal generated at the transmitter, respectively. The signal spectrum is contained in 2 kHz of bandwidth. The signal eye pattern is clear and reasonably free from interference. The slight amount of ISI observed in

POWER SPECTRUM

←———— 5 kHz ————→

FREQUENCY
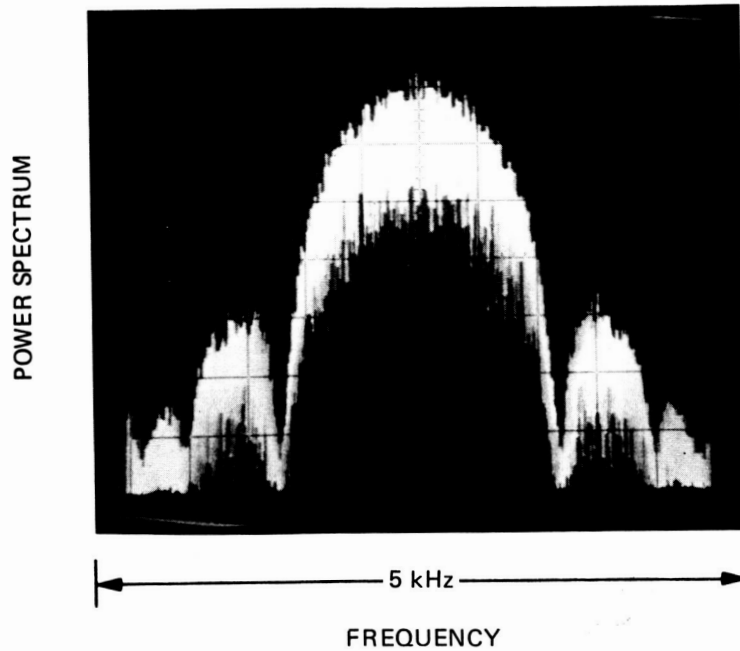
VERTICAL SCALE: 10 dB/div

BIT RATE: 2400 bps

Figure 27. Measured raised-cosine QPSK
signal spectrum.

←——— 2 ms ———→

TIME
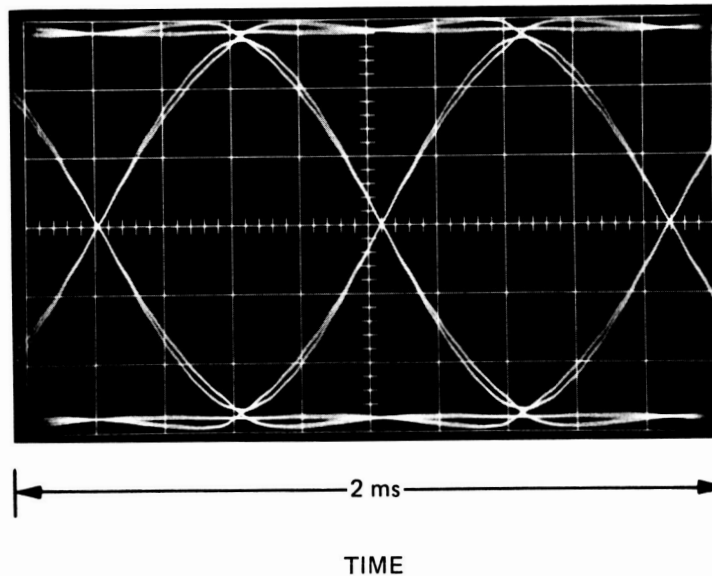
Figure 28. Eye pattern of the raised-cosine
QPSK signal.

Fig. 28 is due to two factors: pulse waveform truncation, and the sample and
hold (instead of sampling alone) operation.

Comparison of Figs. 23 and 27 demonstrates the versatility of the
transmitter. These vastly different spectra can be generated with the flip of
a switch. The eye patterns corresponding to Figs. 23 and 27 are shown in
Figs. 22 and 28, respectively.

VII. MEASURED RECEIVER PERFORMANCE AND
HARDWARE INDUCED DISTORTIONS

The block diagram of Fig. 8 was fabricated to evaluate the performance of a TCT/QPSK modem in the presence of noise and fading. The objectives of the evaluation were to measure the bit error rate, to determine the optimum ratio between the tone power and the signal power, and to examine the receiver error floor. Although the measured error performance in thermal noise and the optimum tone to signal power ratio were very close to that predicted by theory, an error floor not predicted by theory was observed. This error floor is shown (in Section VII.B) to be due to implementation imperfections, which can only be avoided using a digital approach rather than the analog approach used here. For signal transmission, the modulator described in Section VI was used, which provides near-perfect carrier modulation.

The challenges encountered in developing the TCT receiver were:

1.   Implementation of equal delays in the arms of the receiver as well as the PLPF filters.

2.   Implementation of equal gain for the two arms of the receiver.

3.   Signal dividers with large dynamic range.

4.   Implementation of flat gain and group delay response for PLPF filters.

Of the four, the first was the most difficult to resolve.

A.   EXPERIMENTAL RESULTS

Figure 29 demonstrates the existence of an imbalance in the receiver. Figure 29-a shows the eye diagram of the in-phase and quadrature signals (signals Z_i and Z_q of Fig. 8) when only the in-phase signal is transmitted. Figure 29-b shows the eye diagram when only the quadrature signal is transmitted. A cross talk effect is observed in both figures. The efforts to balance the receiver finely enough to eliminate the cross talk were unsuccessful because of the limited flexibility that analog circuitry provides. It is strongly felt that digital implementation of the receiver can easily avoid the cross talk anomaly.

Figure 30 shows the effect of tone calibration, where Fig. 30-a shows the in-phase and quadrature eye diagrams at the transmitter and Fig. 30-b shows the same diagrams reconstructed at the receiver with random data transmission (PN sequence). Figure 31 shows the quadrature signal eye diagram at the receiver in the presence of a 50-Hz frequency offset. The upper trace shows the signal before calibration and the lower trace shows the signal after calibration.

Figure 32 shows the effect of calibration in the presence of Rician fading. In this figure, Doppler frequency is 72 Hz and the specular to multipath ratio, K, is 10. Here again the upper trace is the in-phase signal and the lower trace is the quadrature signal. Similar eye diagrams are shown
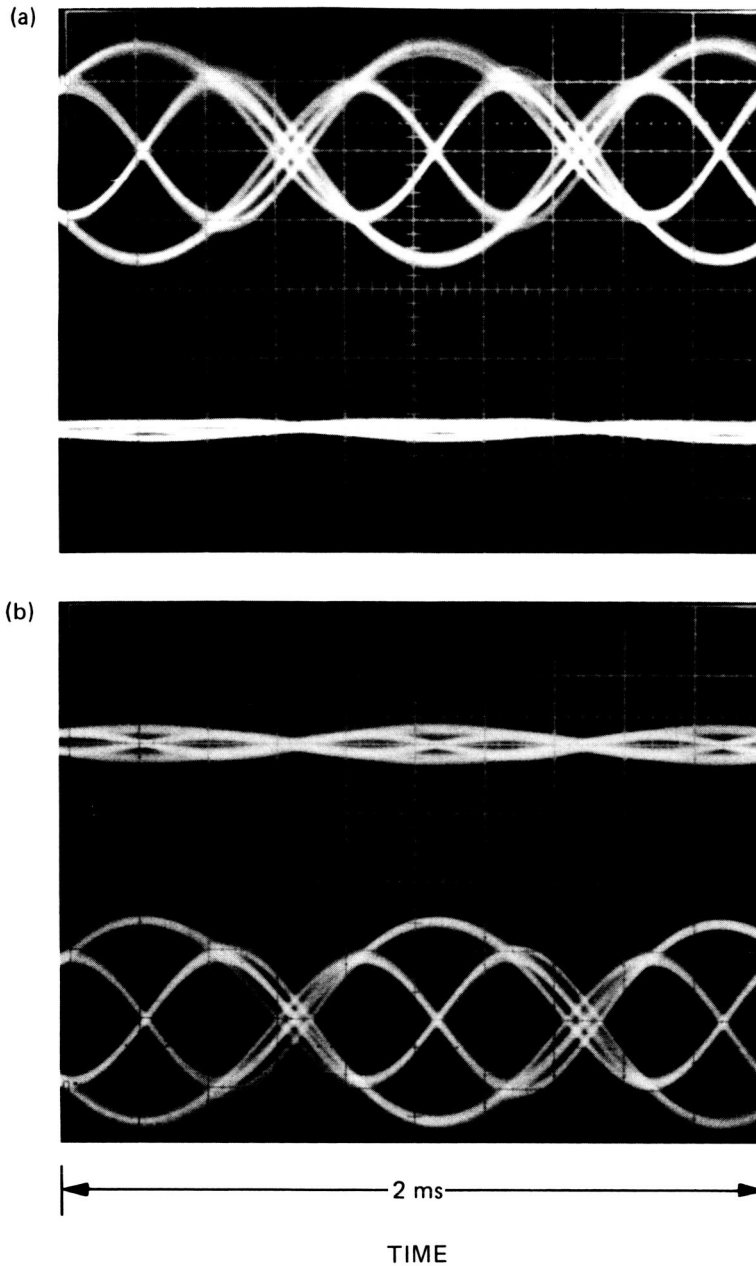
(a)

(b)

2 ms

TIME

BIT RATE: 2400 bps

VERTICAL SCALE: 1 volt/div

UPPER TRACE: I CHANNEL

LOWER TRACE: Q CHANNEL

Figure 29. Cross talk in calibrated outputs.
(a) Feedthrough from in-phase channel
to quadrature channel. (b) Feed-
through from quadrature channel to
in-phase channel.
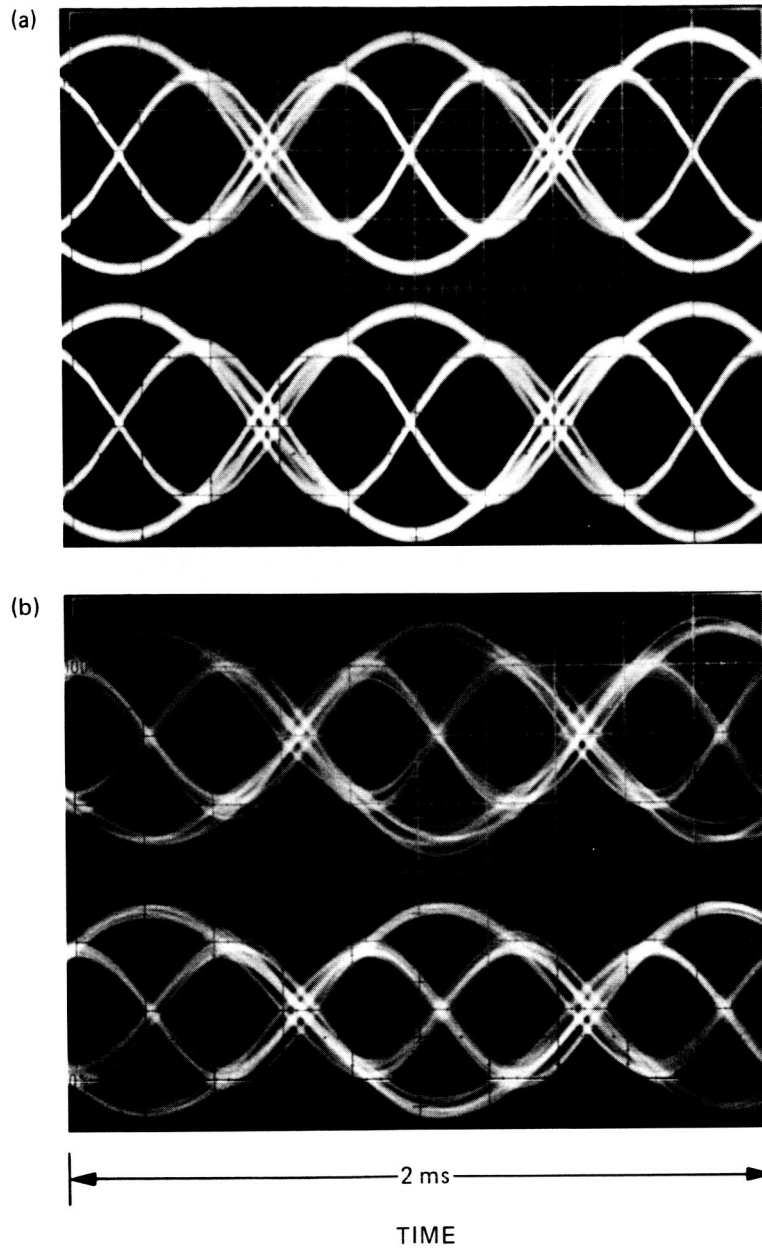
(a)

(b)

|←————————— 2 ms —————————→|

TIME

BIT RATE: 2400 bps

VERTICAL SCALE: 1 volt/div

UPPER TRACE: I CHANNEL

LOWER TRACE: Q CHANNEL

Figure 30. The effect of tone calibration.
(a) Transmitter eye diagram.
(b) Reconstructed eye diagram at
the receiver.

2 ms
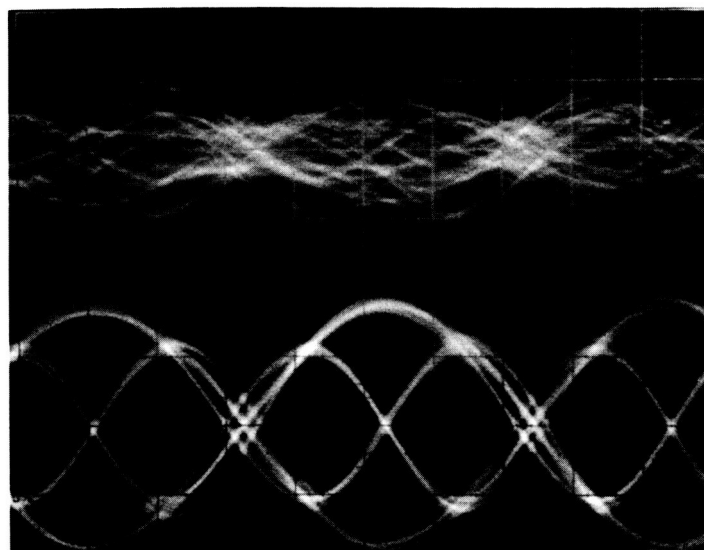
TIME

BIT RATE: 2400 bps

FREQUENCY OFFSET: +50 Hz

UPPER TRACE: UNCALIBRATED Q CHANNEL

VERTICAL SCALE: 2 volts/div

LOWER TRACE: CALIBRATED Q CHANNEL

VERTICAL SCALE: 1 volt/div

Figure 31.   Eye diagram in the presence of a
50-Hz frequency offset.

in Fig. 33 for a Rayleigh fading signal. Figure 34 shows the Rayleigh fading
(Doppler shift is 72 Hz) quadrature signal trace when modulation is off, i.e.,
only carrier present. The lower trace shows the signal without calibration and
the upper trace shows the signal after calibration. Figure 35 shows the same
scenario for the in-phase channel. Due to the existing imbalances in the
receiver, signal calibration on the in-phase waveform is less successful than
the quadrature waveform. In Figs. 34 and 35, the calibrated signals have
higher gains then the uncalibrated ones.
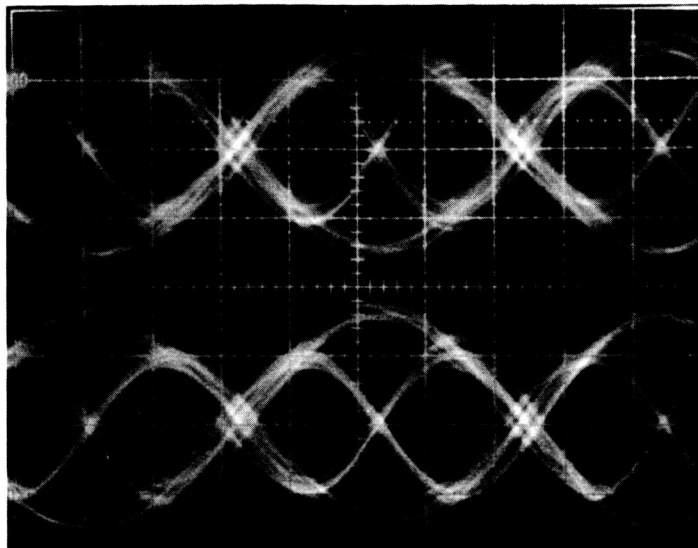
|← ———————— 2 ms ———————— →|

TIME

BIT RATE: 2400 bps

VERTICAL SCALE: 1 volt/div

UPPER TRACE: I CHANNEL

LOWER TRACE: Q CHANNEL

RICIAN FADING WITH F_D = 72 Hz

K = 10 dB

Figure 32. Result of calibration in the
presence of Rician fading.

├────────────────── 2 ms ──────────────────┤

TIME
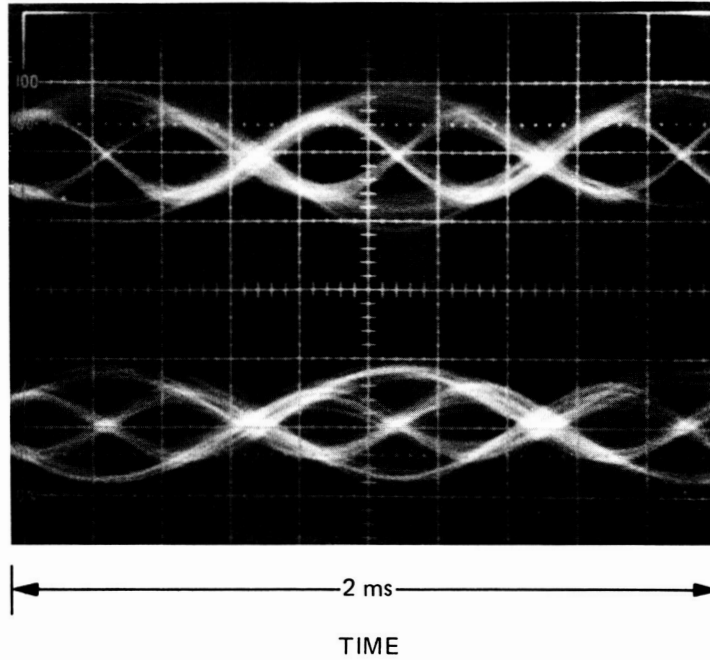
BIT RATE: 2400 bps

VERTICAL SCALE: 2 volt/div

UPPER TRACE: I CHANNEL

LOWER TRACE: Q CHANNEL

RAYLEIGH FADING WITH F_D = 20 Hz

K = 10 dB

Figure 33.　Result of calibration in the presence of Rayleigh fading.
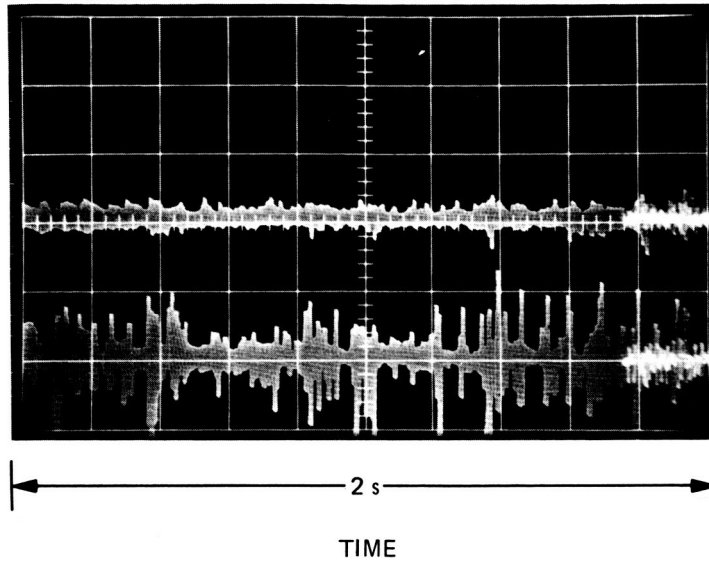
TIME

RAYLEIGH FADING WITH F_D = 72 Hz

UPPER TRACE: CALIBRATED Q CHANNEL

VERTICAL SCALE: 2 volts/div

LOWER TRACE: UNCALIBRATED Q CHANNEL

VERTICAL SCALE: 0.5 volts/div

Figure 34. Result of calibration in the
quadrature channel when modulation
is off (only carrier is present).
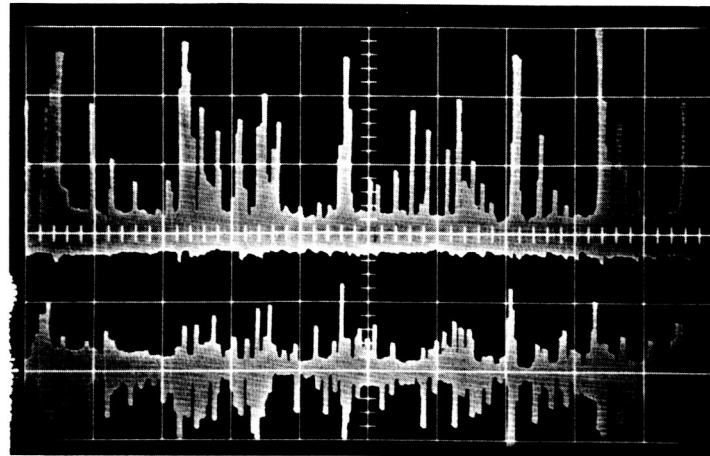
RAYLEIGH FADING WITH F_D = 72 Hz
UPPER TRACE: CALIBRATED I CHANNEL
VERTICAL SCALE: 2 volts/div
LOWER TRACE: UNCALIBRATED I CHANNEL
VERTICAL SCALE: 0.5 volts/div

Figure 35.   Result of calibration in the in-phase channel when modulation is off (only carrier is present).

Figure 36 shows the response of the pilot low pass filter(s). Because a full raised-cosine pulse shaping filter with 50 percent excess bandwidth was used at the transmit end, the receiver matched filter(s) is approximated by a brick-wall filter with its response shown in Fig. 37. Since the transmitted symbol rate is 1200 bps, the cutoff frequency of this filter is 1800 Hz. A 1.8 dB loss is expected because the full filter is placed at the transmit end rather than being shared at the two ends of the link.

FILTER TYPE: BESSEL (NORMALIZED
              TO -3 dB BANDWIDTH)
FILTER ORDER: 9
CUTOFF FREQUENCY: 80 Hz
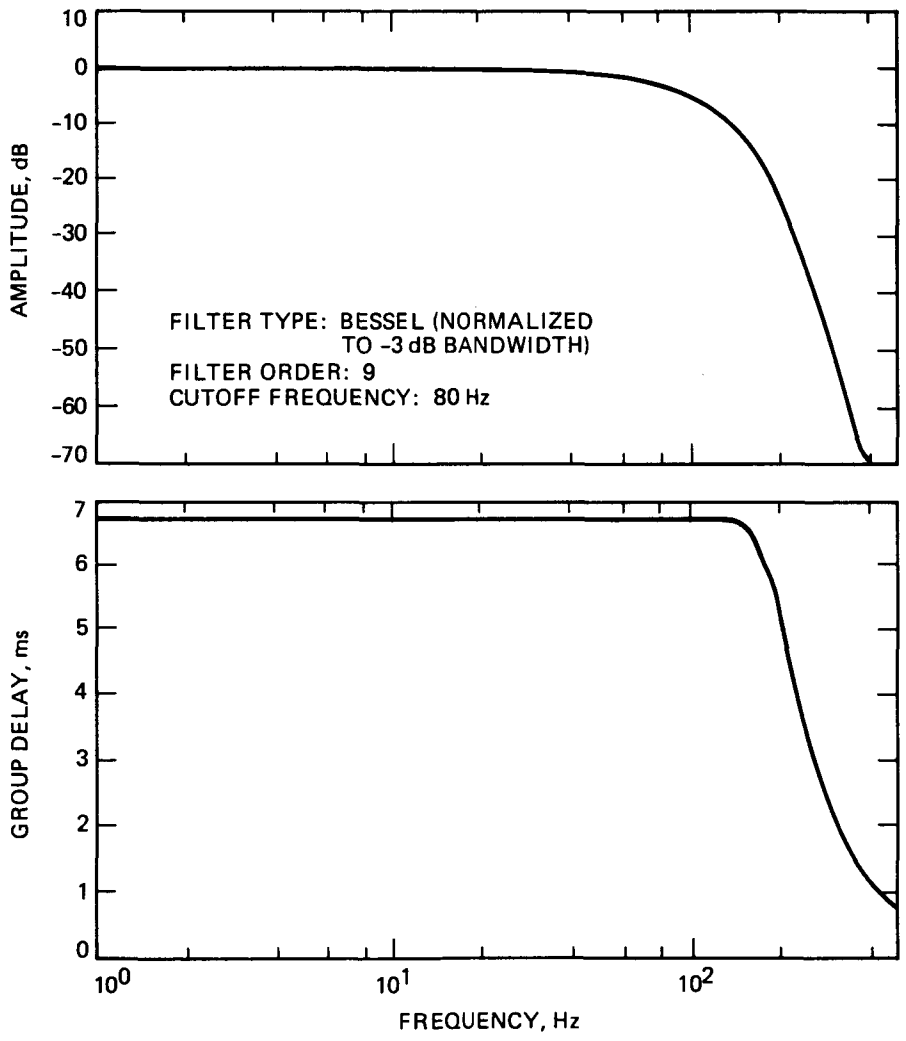
Figure 36. Amplitude and group delay responses of the PLPFs.
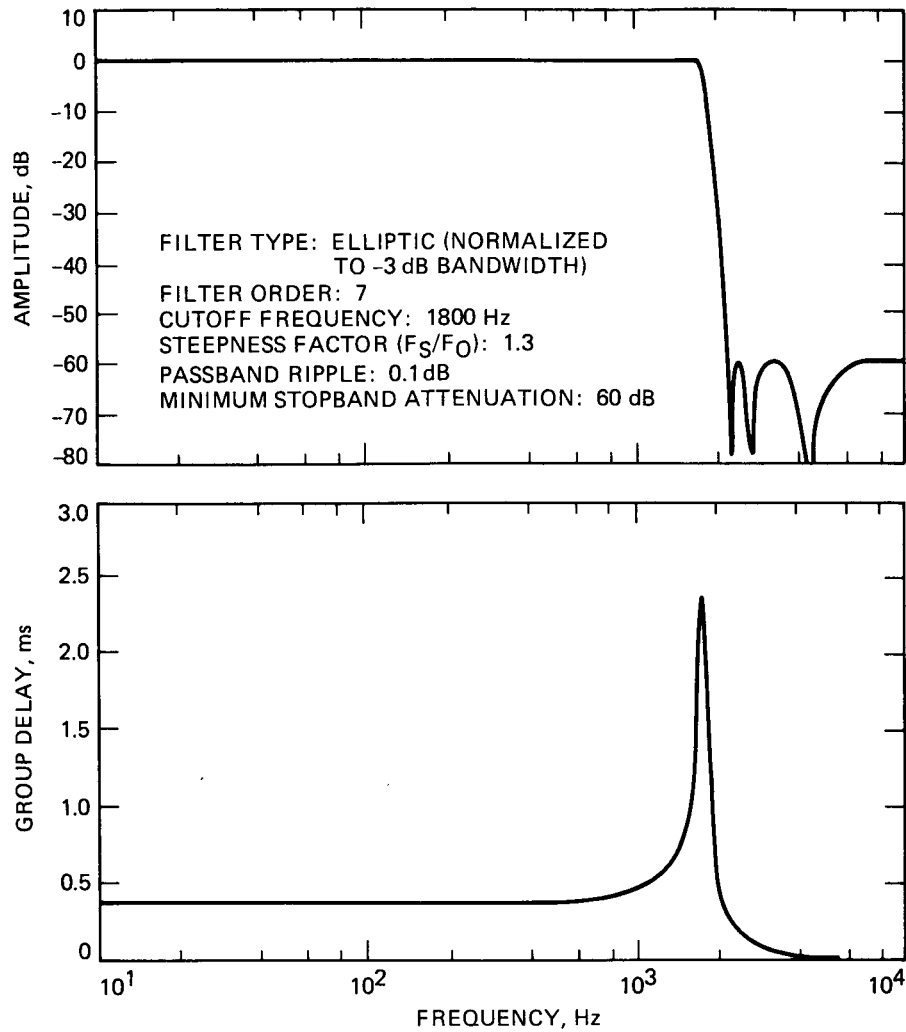
Figure 37. Amplitude and group delay responses of the brick-wall filters.

To evaluate the receiver performance in the presence of noise, the receiver error rate was measured. For a bit rate of 2400 bps, and PLPF bandwidth of 80 Hz, the optimum tone power is analytically computed at 5.5 dB below data power. Using this ratio Fig. 38 is obtained, where the error rate as a function of total bit energy to noise power density (E_T/N_o) is shown. The solid curve shows the theoretical result while the curve with circles shows the measured result. Close agreement between theory and practice is evident. Figure 39 shows the same error rate when two different tone to data power ratios are selected. Clearly, the receiver performance has degraded.
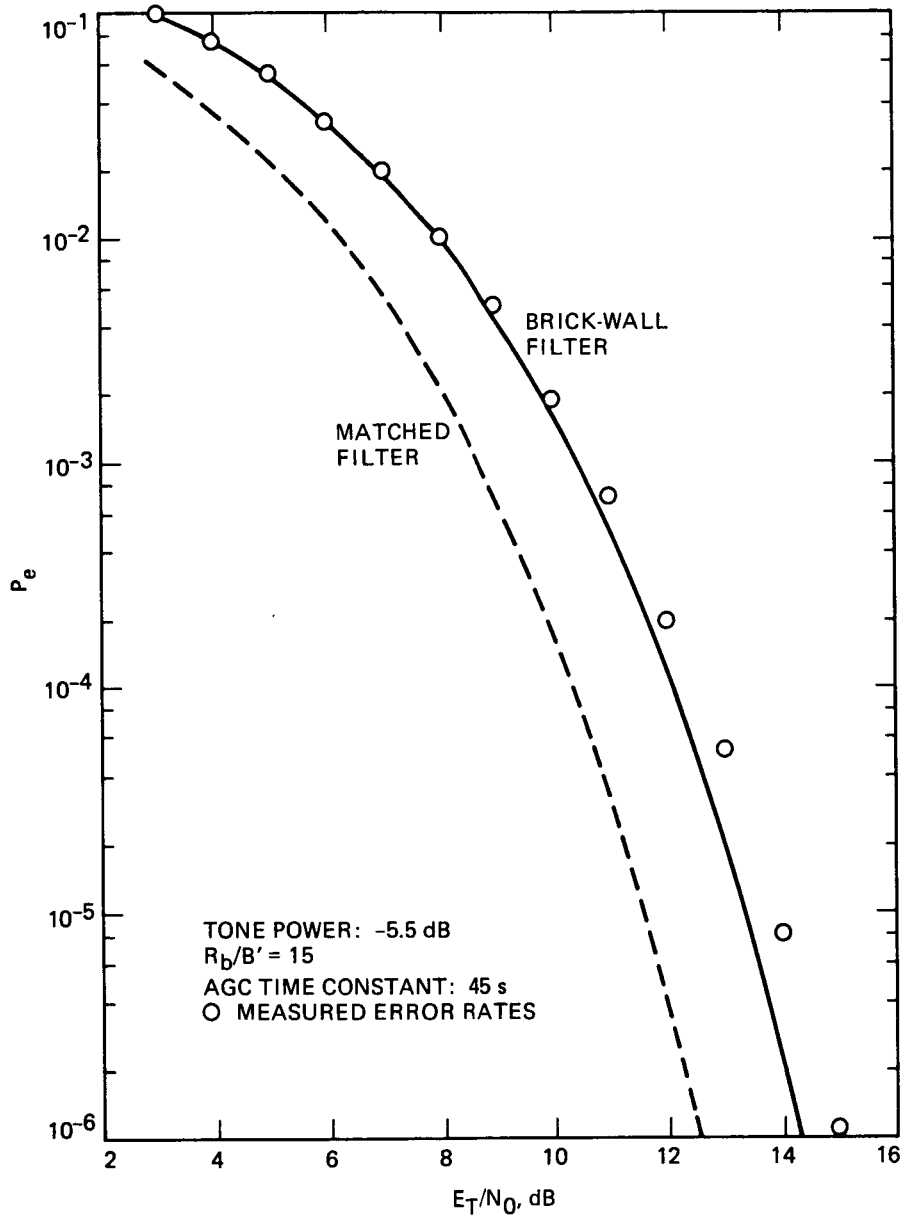
Figure 38. Measured receiver bit error rate in the presence of thermal noise.
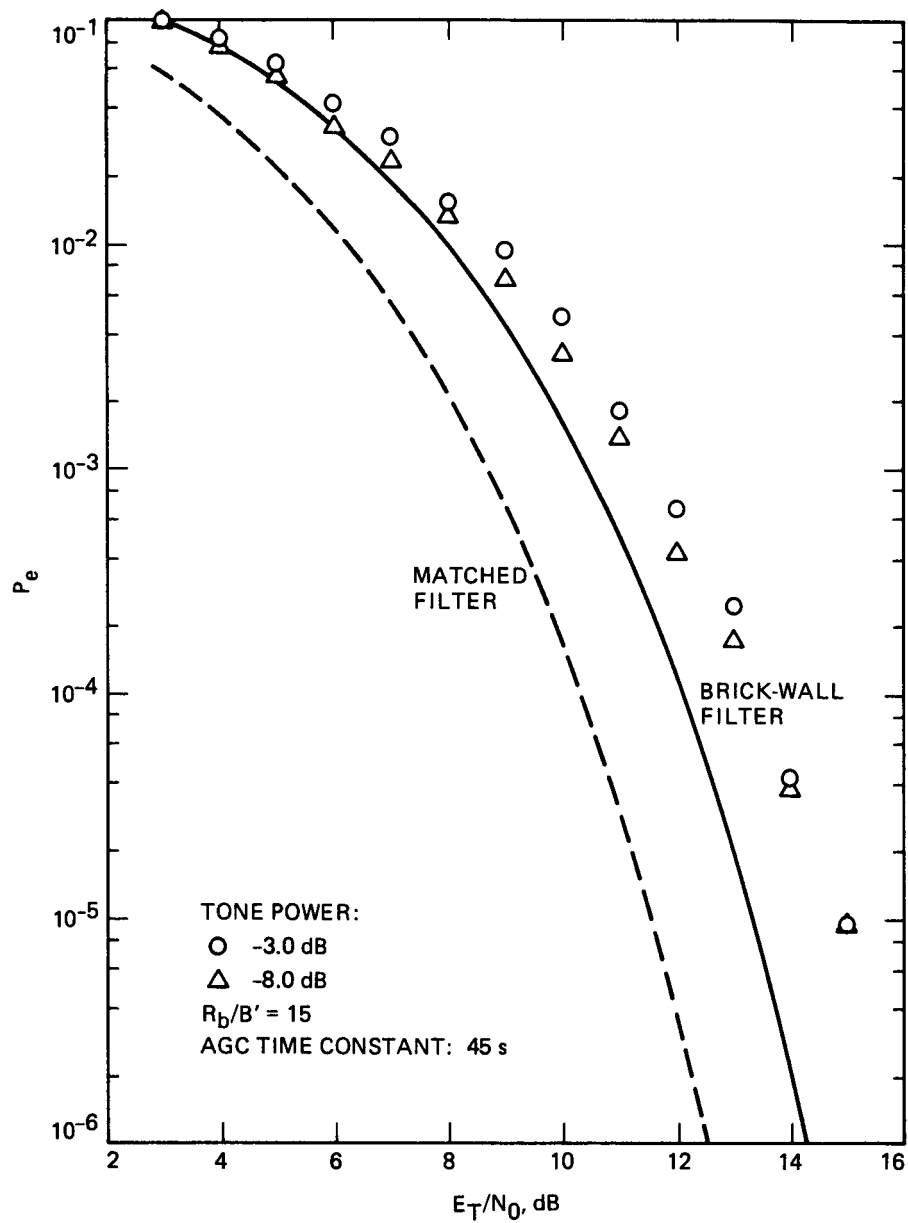
Figure 39. The effect of suboptimal tone-to-data power ratio on the receiver bit error rate.

Figure 40 shows the measured error rate in the presence of a 50-Hz frequency error. Figure 41 shows the measured error rate in the presence of Rayleigh and Rician fading and noise where the fading rate is 20 Hz. These results deviate from theory in the sense that an error floor not predicted by theory is present. The reason for this discrepancy lies in the hardware and it is addressed in the next section. Similar effect is observed in Fig. 42 where the fading rate is increased to 72 Hz. In the above two figures K = 10.
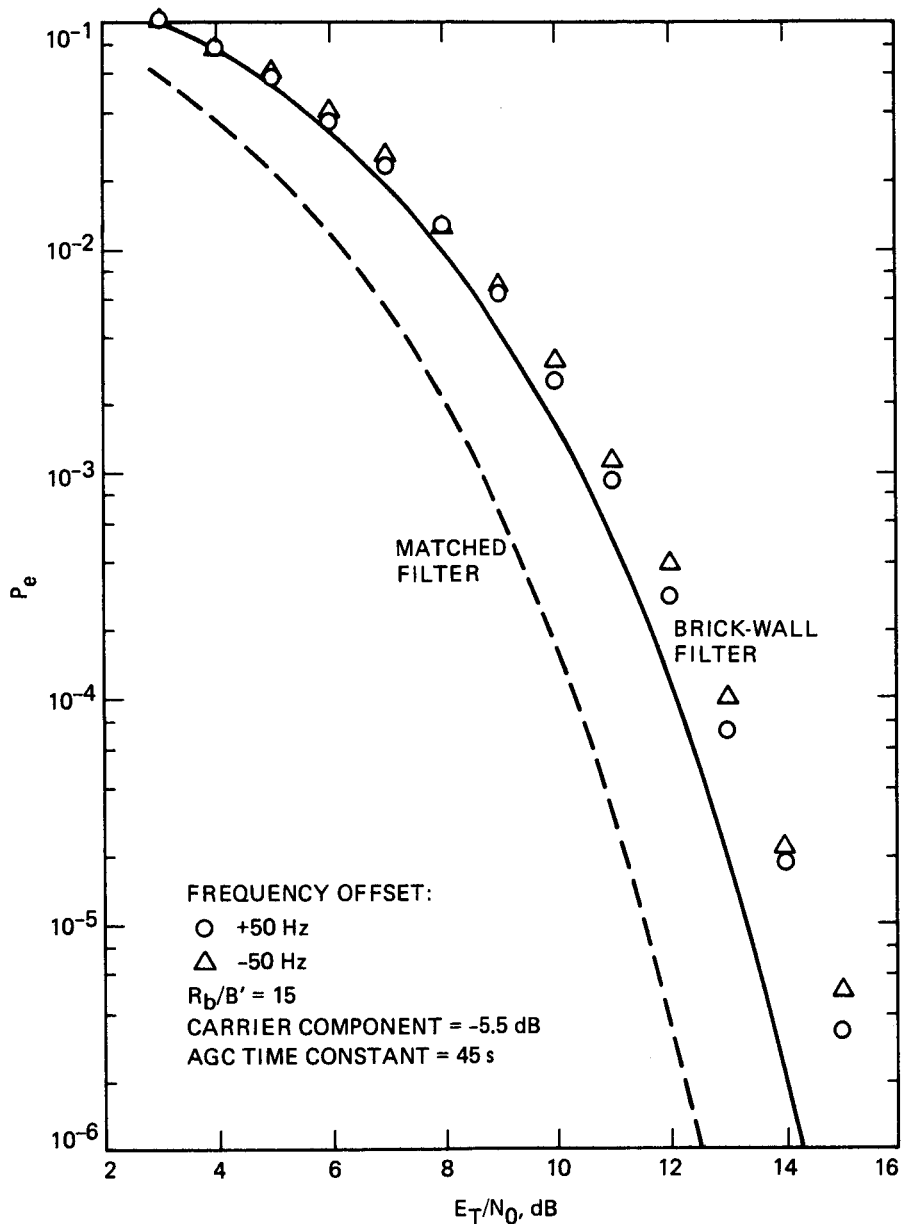
Figure 40. The effect of frequency offset (50 Hz) on the bit error rate.
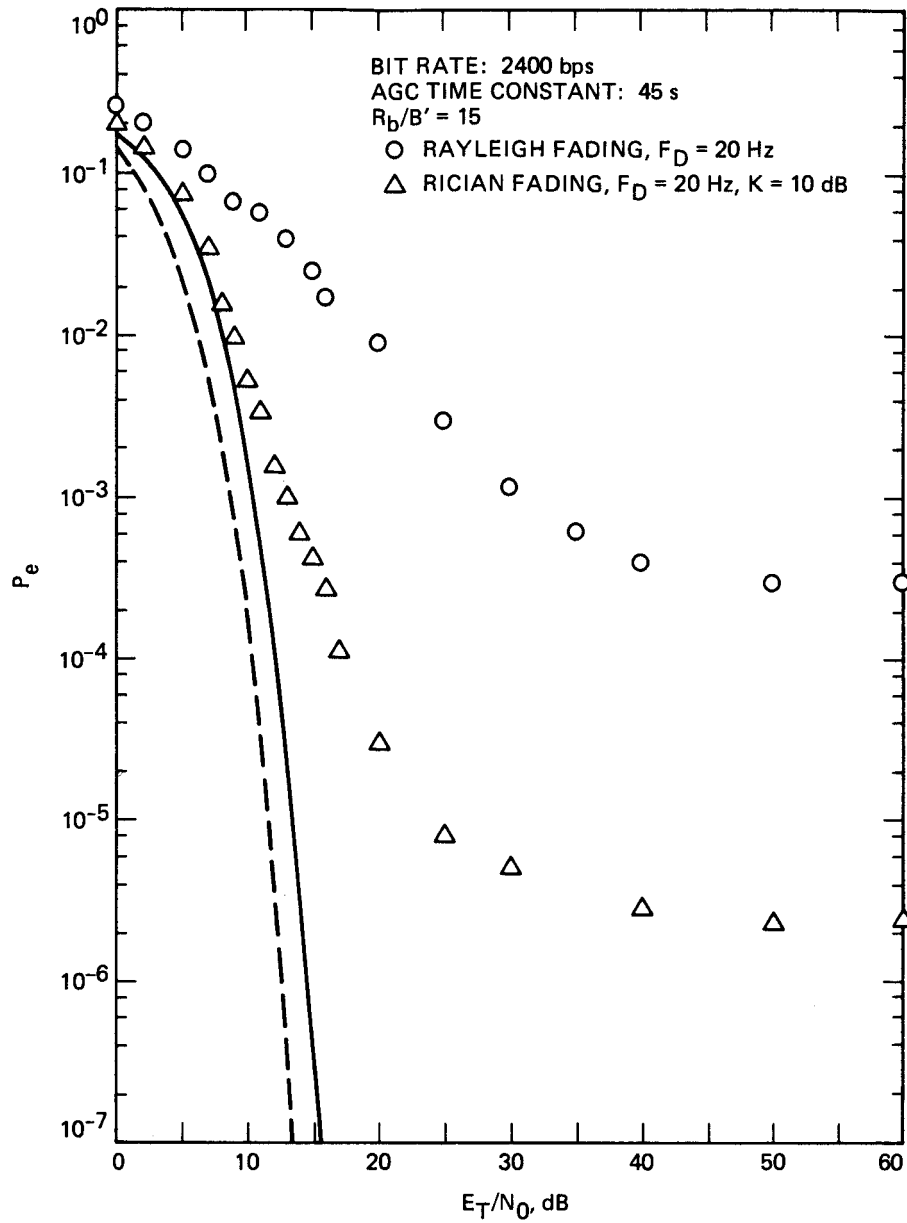
Figure 41. Measured error rate in the presence of Rician and Rayleigh fading with Doppler frequency of 20 Hz.
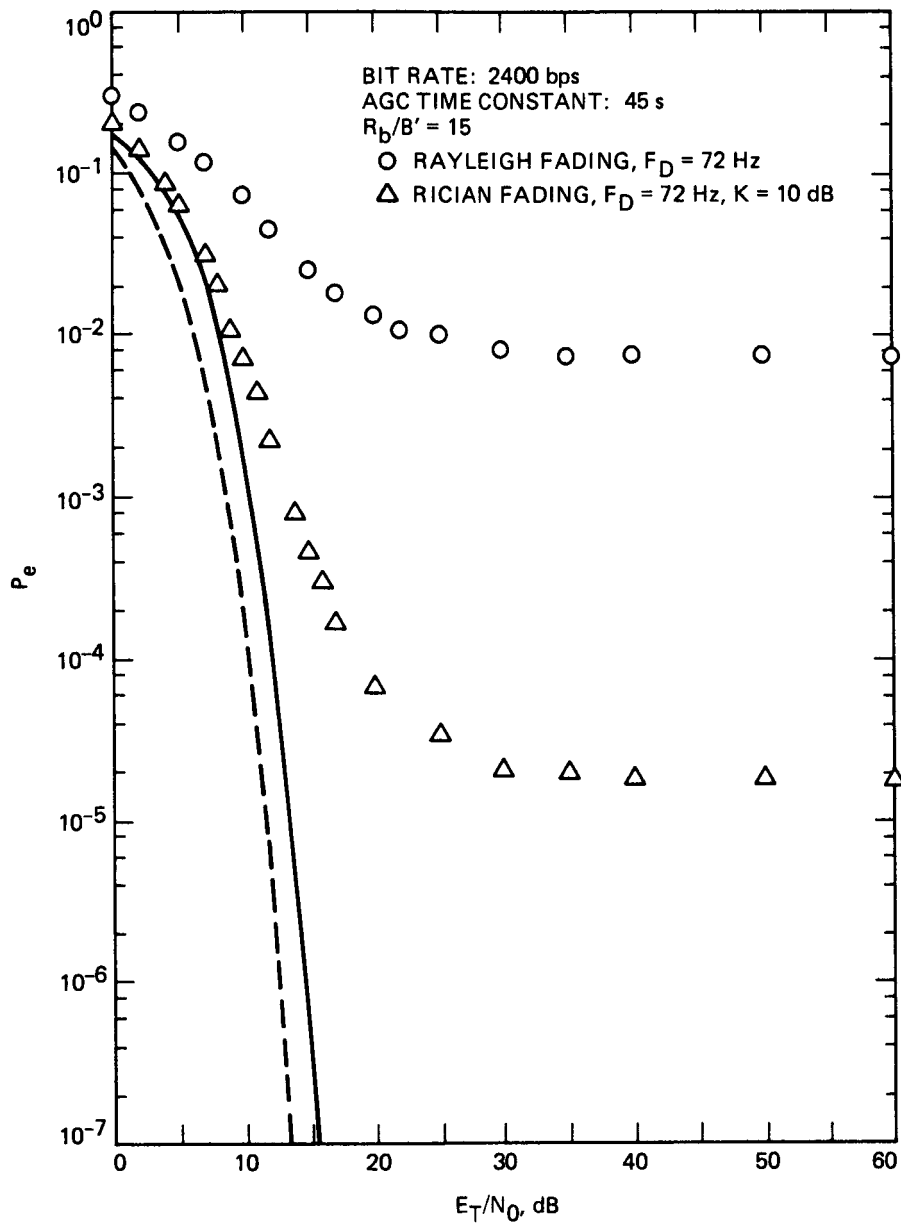
Figure 42. Measured error rate in the presence of Rician and Rayleigh fading with Doppler frequency of 72 Hz.

B.   A BRIEF ANALYSIS OF HARDWARE DISTORTION EFFECTS

The purpose of this section is to examine the performance of the QPSK/TCT receiver in the presence of delay or gain mismatch. In the analysis presented, it is assumed that thermal noise is absent.

1.   DELAY MISMATCH

Let δ denote the delay mismatch between signals $W_i(t)$ and $U_i(t)$ as well as the one for signals $W_q(t)$ and $U_q(t)$[1]. Referring to Fig. 8, in the absence of noise we may write

$$U_i(t) = X(t - \delta) \cos [Y(t - \delta)]$$

$$U_q(t) = X(t - \delta) \sin [Y(t - \delta)]$$

where $W_i(t)$ and $W_q(t)$ are the same as in Eq. (16). The in-phase demodulated signal is given by

$$Z_i(t) = \frac{1}{2X^2(t - \delta)} [W_i(t)U_i(t) + W_q(t)U_q(t)]$$

or

$$Z_i(t) = \frac{X(t)X(t - \delta)}{2X^2(t - \delta)} \left\{ (\cos [Y(t)] \cos [Y(t - \delta)] + \sin [Y(t)] \sin [Y(t - \delta)] \right\}$$

$$+ \frac{X(t)X(t - \delta)}{2X^2(t - \delta)} \left\{ (S_i(t) \cos [Y(t)] \cos [Y(t - \delta)] \right.$$

$$+ S_q(t) \sin [Y(t)] \cos [Y(t - \delta)]$$

$$+ S_i(t) \sin [Y(t)] \sin [Y(t - \delta)]$$

$$\left. - S_q(t) \cos [Y(t)] \sin [Y(t - \delta)] \right\}$$

or

$$Z_i(t) = \frac{X(t)}{2X(t - \delta)} \cos [Y(t) - Y(t - \delta)] \qquad (25)$$

$$+ \frac{X(t)}{2X(t - \delta)} \left\{ (S_i(t) \cos [Y(t) - Y(t - \delta)] \right.$$

$$\left. + S_q(t) \sin [Y(t) - Y(t - \delta)] \right\}$$

---

[1]The case of different delays in the two arms is not addressed.

For ideal time delay equalization, $\delta = 0$ in Eq. (25). In this case:

$$Z_i(t) = \frac{1}{2}[1 + S_i(t)] \tag{26}$$

To determine the potential cross talk between the in-phase and quadrature signals, $S_i(t)$ is set to zero in Eq. (25) to yield the following equation:

$$Z_i(t) = \frac{X(t)}{2X(t - \delta)}\left\{ \cos[Y(t) - Y(t - \delta)] \right. \tag{27}$$

$$\left. + S_q(t) \sin[Y(t) - Y(t - \delta)] \right\}$$

The first term in the above equation (the cosine function) is due to the pilot tone, and the second term (the sine function) is the cross talk—the leakage of the quadrature channel into the in-phase channel. This cross talk is a function of frequency mismatch between the transmitter and the receiver. In the absence of fading, $Y(t)$ can be written as

$$Y(t) = \Delta\omega t + \phi \tag{28}$$

where $\Delta\omega$ denotes the frequency error and ϕ is a constant phase. In the absence of fading, Eq. (27) can be modified as

$$Z_i(t) = \frac{1}{2}[\cos(\Delta\omega\delta) + S_q(t)\sin(\Delta\omega\delta)] \tag{29}$$

Clearly the cross talk is maximized if $\Delta\omega\delta = K\pi/2$, where K is an integer. In practice since δ is small, the cross talk resulting from a delay error is very small.

To examine the effectiveness of calibration on the pilot tone in the presence of fading, $S_q(t)$ is set to zero in Eq. (27). Hence,

$$Z_i(t) = \frac{X(t)}{2X(t - \delta)}\cos[Y(t) - Y(t - \delta)] \tag{30}$$

The argument of the cosine in the above equation is small most of the time. Because of fading the argument becomes large once in a while in a random fashion. This argument will seldom exceed $\pi/2$ if δ is small. The ratio that multiplies the cosine term is always nonnegative. In moments of deep fades this ratio can become very small or very large because $X(t)$ and $X(t - \delta)$ can have substantially different magnitudes in a deep fade situation. Since the cosine term stays positive most of the time, it is expected that the trace of the above signal (pilot tone) will be positive (one-sided). Figure 43 shows the trace of the above function on the scope. This trace is probably affected by other anomalies as well.

It can be shown that the pilot tone in the quadrature channel is given by an equation similar to Eq. (30) with the cosine replaced by a sine and the

TIME
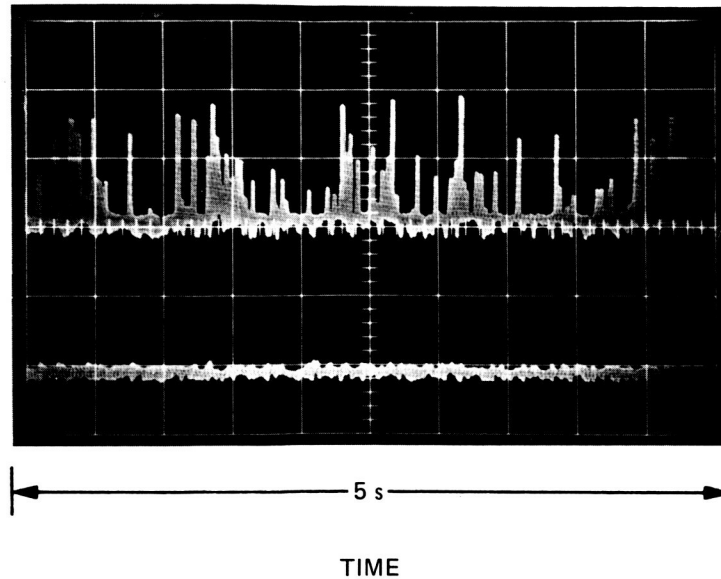
UPPER TRACE: IN-PHASE CHANNEL

LOWER TRACE: QUADRATURE CHANNEL

Figure 43. Calibrated received signal in the
presence of Rayleigh fading with
Doppler frequency at 20 Hz when
modulation is off (carrier only).

argument multiplied by −1. In this case, it is expected that the signal
fluctuations due to fading will be two-sided since the sine function has odd
symmetry about zero. Figure 43 also shows the trace of this signal where
anomalies other than delay error are probably present. The fluctuations are
symmetric, however, they are much smaller than the signal in the in-phase
channel.

2. EFFECT OF ASYMMETRIC GAIN

In this section, it is assumed that the receiver arm delays are matched
but the two arms do not have equal gains. The following equation describes
$Z_i(t)$ for this situation:

$$Z_i(t) = \frac{1}{2} (1 + \varepsilon \sin^2[Y(t)]) + \frac{1}{2} S_i(t) (1 + \varepsilon \sin^2[Y(t)])$$

$$- \frac{\varepsilon}{4} S_q(t) \sin [2Y(t)] \tag{31}$$

where ε denotes the voltage gain difference at the inputs of the summer in
the in-phase channel (see Fig. 1). To examine the cross talk effect, $S_i(t)$
is set to zero resulting in

$$Z_i(t) = \frac{1}{2} (1 + \varepsilon \sin^2[Y(t)]) - \frac{\varepsilon}{4} S_q(t) \sin [2Y(t)] \tag{32}$$

7-18

The cross talk is represented by the last term in the above equation. In the absence of fading, Y(t) is given by Eq. (28). Hence using Eq. (28) in Eq. (32) results in

$$Z_i(t) = \frac{1}{2} [1 + \varepsilon \sin^2(\Delta\omega t + \phi)] + \frac{\varepsilon}{4} S_q(t) \sin (2\Delta\omega t + 2\phi)$$

Hence a cross talk proportional to ε is present.

The success of calibration on the pilot tone can be examined by setting both $S_i(t)$ and $S_q(t)$ equal to zero in Eq. (31):

$$Z_i(t) = \frac{1}{2} + \frac{\varepsilon}{2} \sin^2[Y(t)]$$

or

$$Z_i(t) = \frac{1}{2} + \frac{\varepsilon}{4} - \frac{\varepsilon}{4} \cos [2Y(t)]$$

The above equation indicates that a gain error causes a sinusoid fluctuation around the DC value of $1/2 + \varepsilon/4$. Such fluctuations are small in amplitude if the gain error ε is small. If ε_0 denotes the gain offset in the quadrature channel, the signal component due to the pilot tone in this channel is given by

$$Z_q(t) = \frac{\varepsilon_0}{4} \sin [2Y(t)]$$

Here again a low level fluctuation is observed. No DC exists for this case.

3.   THE ERROR FLOOR ISSUE

Equation 25 indicates that the potential for a bit error exists whenever

$$Y(t) - Y(t - \delta) > \pi/4.$$

The error probability diminishes as δ approaches zero. If δ is on the order of the bit time, an error floor similar to the one observed for DMSK (Refs. 4 and 20) will be present.

At a bit rate of 2400 bps, the bit time is about 0.4 ms. The resolution of the delay line used in the laboratory experiment is about 0.07 ms. This suggests the possibility of an error floor similar to the one observed with DMSK.

Equation 31 shows that no error potential exists for a small gain error.

C. COMMENTS

To control the error floor in a TCT receiver, it is important to reduce the delay error to a negligible level. To eliminate cross talk, both the delay error and gain error must be removed.

In the hardware constructed in our channel simulator laboratory, other potential errors not addressed in this report also exist. An important concern is the two delay lines used to delay match the detected tone with the signals. The oscilloscope traces of the input and output signals to the delay lines show that at times when the signal is faded, the output of the delay line is somehow distorted. Although this distortion is not severe, however, it can be a potential cause of the receiver error floor.

In conclusion, to remedy potential hardware problems, it is suggested that a digital implementation approach be adopted. Using a digital technique, exact delay and gain matching can be achieved. Furthermore, signal delaying can be performed with no added distortion.

REFERENCES

1. S. Carney and D. Linder, "A Digital Mobile Radio for 5-6 kHz Channels," Conference Records, ICC, Philadelphia, PA, p. 5B.3, June 1982.

2. K. Murota and K. Hirade, "GMSK Modulation for Digital Mobile Radio Telephony," IEEE Trans. Communications, Vol. Com-29, pp. 1044-1050, July 1981.

3. M. Simon and C. Wang, "Differential Detection of Gaussian MSK in a Mobile Radio Environment," IEEE Trans. Vehicular Technology, Vol. VT-33, pp. 307-320, November 1984.

4. F. Davarian, M. Simon and J. Sumida, DMSK: A Practical 2400-bps Receiver for the Mobile Satellite Service, JPL Publication 85-51, June 1985.

5. W. Vogel and E. Smith, "Theory and Measurement of Propagation for Satellite to Land Mobile Communications at UHF," Proceedings of 35th IEEE Vehicular Technology Conference, Boulder, CO, May 1985.

6. J. McGeehan and A. Bateman, "Phase-lock Transparent Tone-In-Band (TTIB): A New Spectrum Configuration Particularly Suited to the Transmission of Data Over SSB Mobile Radio Networks," IEEE Trans. Communications, Vol. Com-32, pp. 81-87, January 1984.

7. M. Yokoyama, "BPSK System with Sounder to Combat Rayleigh Fading in Mobile Radio Communications," IEEE Trans. Vehicular Technology, Vol. VT-34, No. 1, February 19, 1985.

8. F. Davarian, "Comments on 'BPSK System With Sounder to Combat Rayleigh Fading'," IEEE Trans. Vehicular Technology, Vol. VT-34, No. 4, November 1985.

9. K. Leland and N. Sollenberger, "Impairment Mechanisms for SSB Mobile Communications at UHF With Pilot-Based Doppler/Fading Correction," Bell System Tech. J., Vol. 59, pp. 1923-1924, December, 1980.

10. J. McGeehan and A. Bateman, "Theoretical and Experimental Investigation of Feedforward Signal Regeneration," IEEE Trans. Vehicular Technology, Vol. VT-32, pp. 106-120, February 1983.

11. W. Jakes, Microwave Mobile Communications. New York: J. Wiley and Sons, pp. 19-22, 1974.

12. F. Davarian, "Imperfect Phase and Timing Transfer Effects on MSK and OQPSK Signals," Proceedings of National Telesystems Conference, Galveston, TX, June 1982.

13. A. Papoulis, Probability, Random Variables and Stochastic Processes. McGraw-Hill, p. 501, 1965.

14. S. Good, "A Comparison of Gaussian Minimum Shift Keying to Frequency Shift Keying for Land Mobile Radio," Proceedings of 34th IEEE Vehicular Technology Conference, Pittsburgh, PA, May 1984.

15. "Tone Calibration for Coherent Reception of Digital Signals in Mobile Channels," prepared for Jet Propulsion Laboratory by General Electric, MSAT Report No. 104, JPL No. 9950-1094, September 1984.

16. S. Good, "An Evaluation of the Tone Calibrated Technique for Data Transmission Over Land Mobile Radio Channels," Proceedings of 35th IEEE Vehicular Technology Conference, Boulder, CO, May 1985.

17. G. Forney, et al., "Efficient Modulation for Band-Limited Channels," IEEE J. Selec. Areas Common., Vol. SAC-2, No. 5, pp. 632-647, September 1984.

18. H. Suzuki and Y. Yamao, "Design of Quadrature Modulator for Digital FM Signaling with Digital Signal Processing," Trans. IECE of Japan, Vol. J65-B, No. 9, pp. 1148-1155, September 1982, [in Japanese].

19. D. Divsalar and M. Simon, "Trellis Coding With Asymmetric Signal Sets," paper presented at IEEE Int. Symposium on Information Theory, Brighton, England, June 1985.

20. F. Davarian and J. Sumida, "2400 bit/s DMSK Modem for Mobile Satellite Service," Electronics Letters, Vol. 21, No. 21, October 1985.

APPENDIX. DATA ENCODING TECHNIQUES

The success of TCT in reaching its power and bandwidth objectives greatly depends on the encoding of the baseband signal. It would be best if the residual carrier power were at a minimum. To accomplish this the received tone has to be free from data-induced interference (self-interference). A coding technique is needed that spreads the data spectrum away from the origin and, hence, creates a null at DC (Ref. 1). It can be shown that a multipath fading tone is bandlimited to twice the Doppler (Ref. 2). Thus, the coding applied to the data must ensure very low power density in a one-sided bandwidth of twice the maximum Doppler shift, to account for both tone and data-bearing signal spectral spreading. On the other hand, overspreading of the signal spectrum results in gross bandwidth expansion, which is also undesirable. The purpose of this appendix is to introduce a suitable coding technique that results in the desired low power band around DC without overspreading of the signal spectrum.

In order to make our discussion manageable, the source rate R is assumed to be one of the following values: 1200, 2400, 4800, 8000, or 32000 bps. A maximum Doppler frequency of d = 78 Hz is considered. Since the biggest challenge is attributed to the lower source rate of 1200, we will concentrate on a Doppler-to-source ratio of 78/1200 = .065 or 6.5 percent.

The coding technique proposed here is a code that results in an equal number of "ones" and "zeros" in the channel symbol stream and, hence, it is called the balanced code. The next section describes how the class of balanced codes is constructed and presents their power spectral density. An evaluation comparing this code with the Miller and Welch codes is also given (Refs. 3 and 4).

The Balanced Code

The balanced technique uses a class of codes in which the code words have an equal number of "ones" and "zeros". This characteristic always guarantees a spectral null at DC regardless of the code length. Construction of this code is performed simply by mapping M source symbols into N channel symbols as described below. First, note that N, which is the code word length, is an even integer; each code word has exactly N/2 "ones" and N/2 "zeros", and N > M. The exact relationship of N to M will be derived shortly. A binary code of length N contains 2^N signals, of which exactly $\dfrac{N!}{\left[(N/2)!\right]^2}$ have an equal number of "ones" and "zeros". Therefore

$$M = \text{Log}_2\left\{\frac{N!}{\left[\left(\frac{N}{2}\right)!\right]^2}\right\} \tag{1}$$

In practice, M is selected to be the largest integer that satisfies

$$M \leq \text{Log}_2\left\{\frac{N!}{\left[\left(\frac{N}{2}\right)!\right]^2}\right\} \tag{2}$$

A-1

Referring to Eq. (1) the code efficiency as a function of N can be written as

$$C(N) = \frac{Log_2 \left\{ \dfrac{N!}{\left[\left(\dfrac{N}{2} \right)! \right]^2} \right\}}{N} \tag{3}$$

For example, $C(2) = .5$, $C(8) = .766$, and it can be shown that the code efficiency approaches 1 as N increases toward infinity. The bandwidth expansion due to coding can easily be computed. Let b(N) denote the bandwidth ratio of the coded data to the uncoded data, then

$$b(N) = \frac{1}{C(N)} \tag{4}$$

For example, for N = 2 (Manchester code) this ratio is 2. For large N, b(N) approaches unity; however, the low interference band around DC also vanishes as N becomes large. Therefore, it appears that for any given Doppler to bit rate ratio, an optimum N exists which results in the minimum bandwidth expansion.

The power spectral density of the balanced code can be determined in closed form (Ref. 5) and is given by

$$\frac{S(f)}{E_s} = \frac{|G(f)|^2}{T_s} \left[\frac{N}{N-1} - \frac{1}{N(N-1)} \frac{\sin^2(N\pi f T_s)}{\sin^2(\pi f T_s)} \right] \tag{5}$$

where E_s, T_s and G(f) denote the channel symbol energy, period and Fourier transform, respectively. An attractive property of the balanced code is that the signal power spectral density as given by Eq. (5) always has a null at the origin regardless of N. The smallest value of N, i.e., N = 2, corresponds to the well-known Manchester code, when the channel symbol, g(t), is a square pulse, which has a reasonably large interference-free band around DC. As N increases, the size of the interference-free band is reduced and in the limit this band becomes only a point at the origin (DC). Notice that for N equal to infinity, the signal power spectrum becomes that of the NRZ code with the exception of a null at the center. The following two equations represent the power spectral densities for the two limiting values of N, respectively.

For N = 2:
$$\frac{S(f)}{E_s} = 2\ \frac{\sin^4(\pi fT_s)}{(\pi fT_s)^2}$$

For N = ∞:
$$\frac{S(f)}{E_s} = \begin{cases} \dfrac{\sin^2(\pi fT_s)}{(\pi fT_s)^2} & \text{for } f \neq 0 \\\\ 0 & \text{for } f = 0 \end{cases} \tag{6}$$

Figure A-1 illustrates the power spectral density of the balanced code for N = 2 and N = 6 as a function of the time-frequency product.
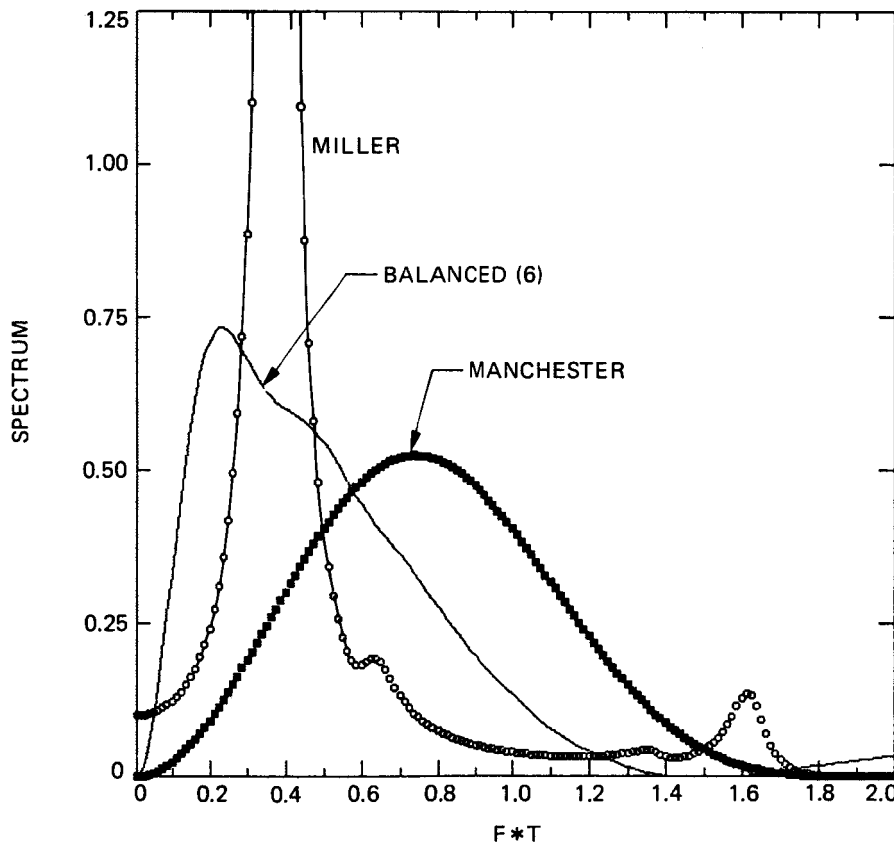

Figure A-1. Power spectral densities of Manchester, balanced (N = 6), and Miller coded waveforms.

Power in a Narrow Bandwidth

The objective of the code studied in this appendix is to ensure very little interference in the tone detection filter of the coherent receiver. As mentioned earlier, the bandwidth of this bandpass filter is, theoretically, equal to twice the maximum Doppler shift. However, in practice, due to practical limitations such as spreading of signal spectrum from fading, it is required that a low interference bandpass region of four times the Doppler exist for successful detection of the tone. Therefore, the one-sided bandwidth, B, of interest is equal to twice the expected maximum Doppler. Since the particular Doppler-to-source ratio may vary from system to system, it appears useful to evaluate the power in a band around DC as a function of the time-bandwidth product for each code. Figure A-2 illustrates the power contained in a bandwidth B for the balanced code as well as the Miller and Welch codes, where the time normalizing factor T is the source bit period.
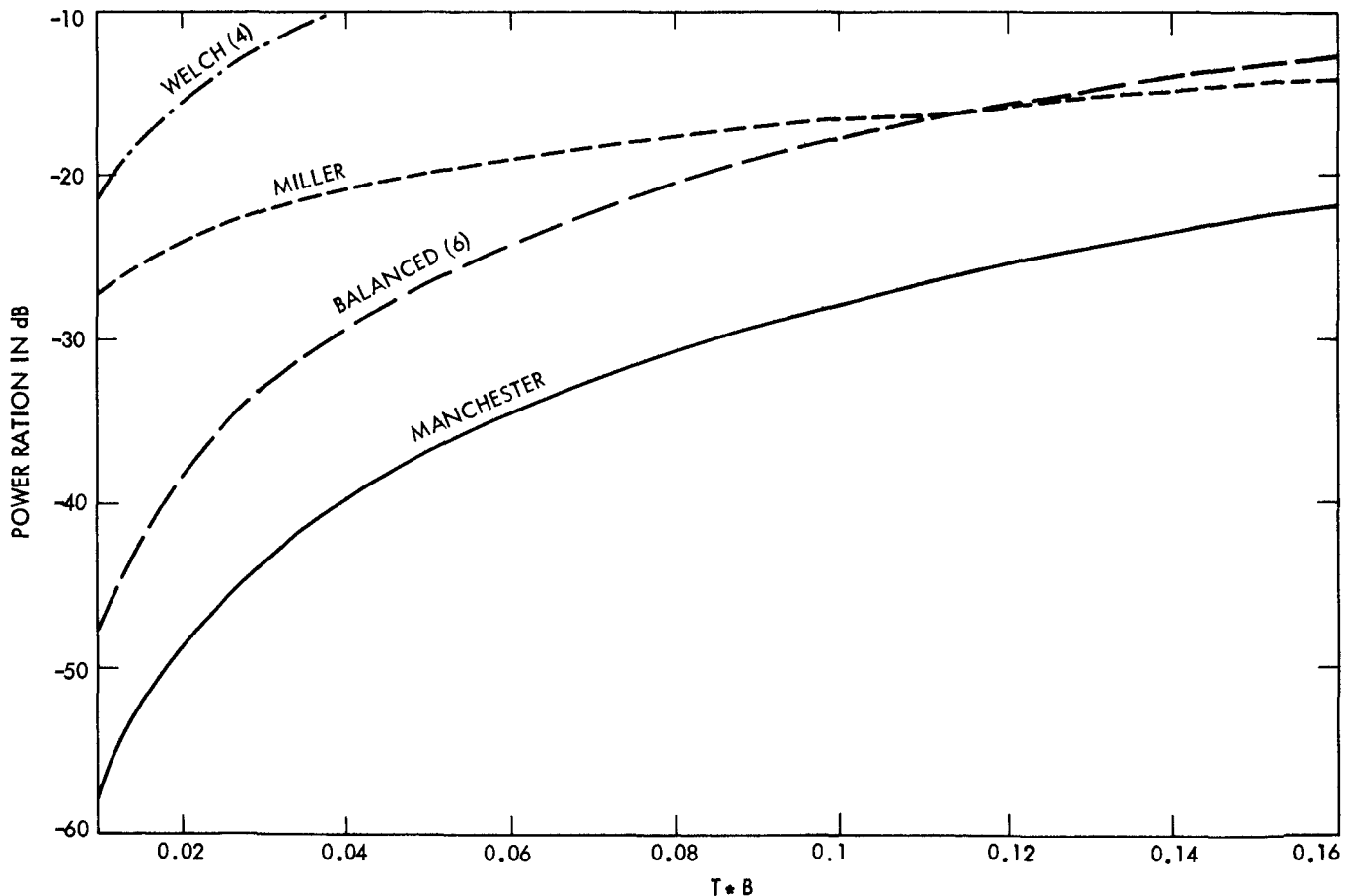

Figure A-2. Power in a given bandwidth for balanced, Manchester, Miller and Welch Codes. The plot for the Welch code represents an upper bound.

The balanced code plot in Fig. A-2 corresponds to N = 6, which results in a 3/2 bandwidth expansion ratio since every 4 source bits are mapped into 6 channel bits. The bandwidth expansion ratio of the Manchester code is 2/1. Also, the expansion ratio associated with the Miller code is between 1 and 2, while the same ratio for the Welch code is 4/3 (every 3 bits are mapped into 4 channel symbols). It is assumed that the NRZ coded data has bandwidth unity. From Fig. A-2 it appears that the lowest interference in a band about DC is produced by the Manchester code followed by the balanced, Miller and Welch codes. Note that for BT > 0.12 the relative order of balanced and Miller codes reverses. There is no power overhead associated with these codes except for the Welch code which suffers from a power loss of 1.25 dB.

Concerning the balanced code, it should be noted that in practice not all the elementary signals in the code book are used. For N = 6 there are 20 elementary signals which have an equal number of "ones" and "zeros" while only 16 of them are necessary to represent 4 bits of information. The power ratio function of Fig. A-2, however, assumes that only "111000" and its complement are left out. In other words, the power ratio curve corresponds to the case where all the elementary signals of length 6, and having an equal number of "ones" and "zeros" are present with equal probability except the pair just mentioned.

Spectral Shaping

In the previous sections it was shown that lowering signal power in a band around DC would result in an expanded signal bandwidth that is unsuitable for spectrum conservation. To remedy this unwanted artifact, appropriate forms of pulse shaping can be employed to reshape the signal spectrum for enhanced spectral utility. Needless to say, the results presented in the previous sections had assumed rectangular pulse shapes. In practice, however, it turns out that this pulse shape is bandwidth inefficient, and hence some form of bandlimiting has to be applied. Although this objective can be reached simply by filtering of the signal at the IF stage, such an approach suffers from power losses due to intersymbol interference. A class of pulse shaping techniques, known as the raised-cosine characteristic (Ref. 6) exists which bandlimits the signal without introduction of intersymbol interference at the sampling time. The raised-cosine characteristic can be constructed using a roll-off factor, which can vary from 0 to 100 percent. The zero roll-off factor results in the minimum bandwidth occupancy and hence is considered here. Clearly, in practice, a small measure of roll-off is necessary for filter implementation reasons. The transfer function of the Nyquist filter under consideration is given as

$$H(f) = \begin{cases} \sqrt{T_s} & \text{for } |f| < \dfrac{1}{2T_s} \\ 0 & \text{otherwise} \end{cases} \tag{7}$$

where, as mentioned earlier, T_s is the channel symbol period, i.e., T_s equals T/2 and 3T/2 for Manchester and the balanced codes (N = 6), respectively.

An application of the above pulse-shaping technique in conjunction with the proposed coding methods will result in a strictly bandlimited signal which also possesses a low interference zone around DC. Figure A-3 depicts the power spectral densities of the Nyquist pulse-shaped signal with Manchester and balanced coding, respectively.
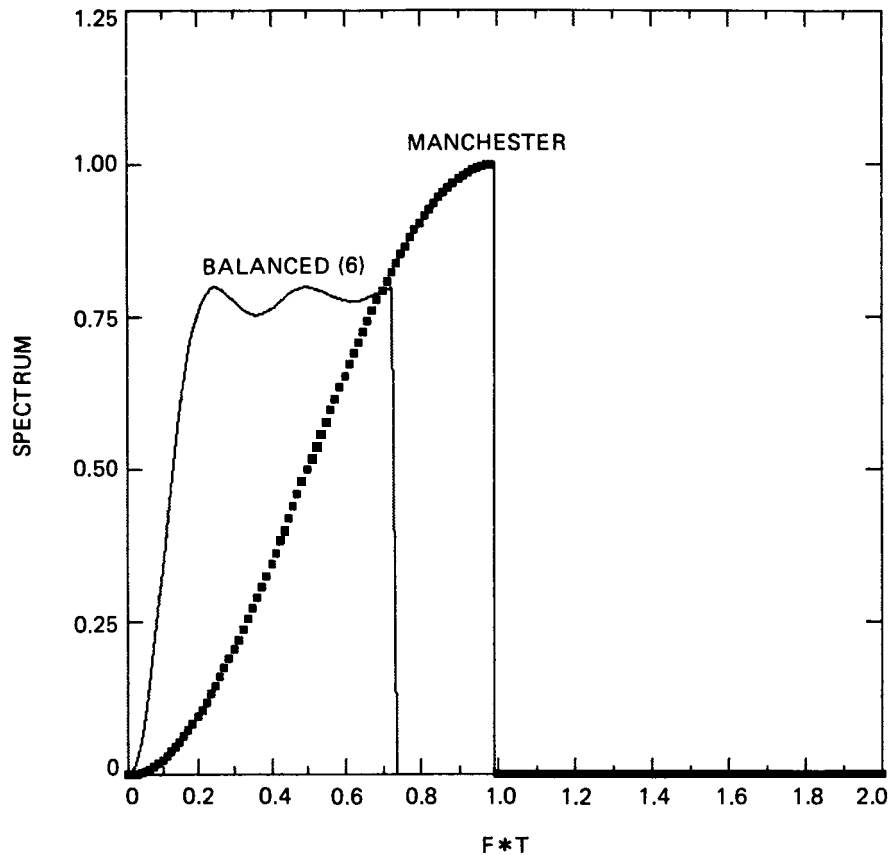
Figure A-3. Power spectral densities of Manchester and balanced (N = 6) coded waveforms with Nyquist pulse shaping.

Discussion

At this point it is useful to run an objective evaluation of the four candidate codes. Let's assume that it is desirable to maintain the in-band signal power at least 20 dB below the total power. Earlier it was pointed out that the largest band of interest is 13 percent of the source bit rate, which corresponds to the lowest bit rate of 1200 bps. It immediately appears from Fig. A-2 that the Welch code, except for the highest bit rate of interest (R = 32000 bps), does not meet the in-band interference requirement. On the other hand, the Manchester code exhibits the lowest in-band interference, however, its bandwidth expansion property makes this code unattractive. Nevertheless, for the lowest bit rate of 1200 bps, this code is the only acceptable one and,

thus, has to be selected for this bit rate. Between the remaining candidates, that is, Miller and balanced, the Miller code is not able to meet the required specification at the next point of interest, i.e., BT = .065 corresponding to R = 2400 bps. For the rest of the region of interest the balanced code clearly outperforms the Miller code. Therefore, it can be concluded that for the present scenario, either the balanced code or the Manchester are the suitable options, that is, Manchester to be used for the lowest source rate and balanced to be used for all other cases.

There are some additional advantages to the balanced code. For example, since some of the legitimate elementary signals will never be used, this fact may be exploited by the receiver to improve the power performance beyond that of BPSK. In essence what this means is that the bandwidth expansion caused by this code may be used to reduce power consumption. The other usefulness of this code is that one of the signals not used may be transmitted periodically to function as a field delimiter or separator, a useful characteristic in a mobile environment. If the source requirements change for higher bit rates, it is possible to utilize a balanced code with length larger than 6 in order to reduce signal bandwidth.

There are two disadvantages to the balanced code. First, this technique adds a delay of M bits (M = 4 for N = 6) to the modulator. Second, this code slightly complicates the receiver structure particularly when decoding strategy tries to maximize power performance. Nevertheless, the added complexity is foreseen to be slight and not a major hindrance.

References

1. F. Davarian, "Satellite-aided Mobile Communications: High Performance Digital Radios," International Communications and Energy Conference Record, Montreal, Canada, pp. 238-243, October 1984.

2. W. Jakes, Microwave Mobile Communications, John Wiley, New York, pp. 19-22, 1974.

3. W. Lindsey and M. Simon, Telecommunication Systems Engineering, Prentice-Hall, New Jersey, p. 18, 1973.

4. L. Welch, "Spectral Shaping Without Subcarriers," Conference Records, ITC, pp. 883-885, 1978.

5. F. Davarian, "Coding Techniques Suitable for Residual Carrier Transmission in Mobile Links," JPL unpublished report, Jan. 1984.

6. R. Lucky, J. Salz and E. Weldon, Principles of Data Communication, McGraw-Hill, pp. 50-51, 1968.